Electron transfer via bridges

M. Bixon and Joshua Jortner

Citation: The Journal of Chemical Physics **107**, 5154 (1997); doi: 10.1063/1.474878
View online: http://dx.doi.org/10.1063/1.474878
View Table of Contents: http://aip.scitation.org/toc/jcp/107/13
Published by the American Institute of Physics

Electron transfer via bridges

M. Bixon and Joshua Jortner
School of Chemistry, Tel Aviv University, Ramat Aviv, Tel Aviv 69978, Israel

(Received 3 February 1997; accepted 29 May 1997)

In this paper we explore the energetic control of sequential and superexchange electron transfer (ET) mechanisms on the basis of quantum-mechanical simulations and calculations for long-range ET in DBA systems, where the donor (D) and the acceptor (A) are separated by a bridge (B). We studied ET dynamics in a Franck–Condon (FC) system characterized by three multi-dimensional displaced harmonic potential surfaces, where an initial single vibronic doorway state $|\alpha\rangle$ (with energy E_α) in the DBA ($\equiv$D) electronic state is coupled to the mediating $\{|\beta\rangle\}$ vibronic quasicontinuum of the D^+B^-A ($\equiv$B) electronic state, which in turn is coupled to the final $\{|\gamma\rangle\}$ vibronic quasicontinuum of the D^+BA^- ($\equiv$A) electronic state. The level structure was described by the vibrational frequencies (for a four-mode harmonic system) and the energy gaps ΔG_{DB} and ΔG_{DA} between the origins of the corresponding electronic states (with $n_\alpha=1-50$, $n_\beta=1000-2000$, and $n_\gamma=1000-2000$ states in the $\{|\alpha\rangle\}$, $\{|\beta\rangle\}$, and $\{|\gamma\rangle\}$ manifolds, respectively), while the couplings were characterized by the spectral densities and by the pair correlations (specified in terms of correlation parameters $\eta_{\alpha\alpha'}$ and $\eta_{\beta\beta'}$) between states belonging to the same manifold. The correlation parameters $\eta_{\alpha\alpha'}$ ($\alpha,\alpha'=1-40$) for the doorway-quasicontinuum coupling and $\eta_{\beta\beta'}$ ($\beta,\beta'=150-190$) for the interquasicontinuum coupling are considerably lower than unity ($|\eta_{\alpha\alpha'}|\leqslant 0.4$ and $|\eta_{\beta\beta'}|\leqslant 0.3$), obeying propensity rules with the highest values of $|\eta_{\alpha\alpha'}|$ and $|\eta_{\beta\beta'}|$ which correspond to a single vibrational quantum difference, while for multimode changes between α and α' or between β and β' very low values of $|\eta_{\alpha\alpha'}|$ or $|\eta_{\beta\beta'}|$ are exhibited. Radiationless transitions theory was applied for quantum-mechanical simulations based on the dynamcis of wave packets of molecular eigenstates for resonance ($\Delta G_{DB}<E_\alpha$) and for off-resonance ($\Delta G_{DB}>E_\alpha$) coupling. Resonance $|\alpha\rangle-\{|\beta\rangle\}-\{|\gamma\rangle\}$ coupling results in two-step sequential ET kinetics for all doorway states $|\alpha\rangle$, manifesting phase erosion due to weakly correlated intercontinuum coupling, without the need of intermediate state phonon induced thermalization. Off-resonance $|\alpha\rangle-\{|\beta\rangle\}$ coupling in conjunction with $\{|\beta\rangle\}-\{|\gamma\rangle\}$ resonance interactions results in unistep superexchange ET kinetics. The simulated sequential ET rates and the superexchange rate are in good agreement with the calculated quantum-mechanical rates obtained using the electronic couplings and FC densities. The energy-gap (ΔG_{DB}) dependence of the simulated and the calculated ET rates from a single doorway state reveal a ''transition'' from sequential to superexchange ET with increasing ΔG_{DB}. For a finite-temperature system, characterized by a fixed ΔG_{DB} (>0) small energy gap, the thermally averaged rate from a canonical ensemble of doorway states will result in the superposition of both superexchange and sequential mechanisms. © *1997 American Institute of Physics.* [S0021-9606(97)01633-4]

I. INTRODUCTION

Electron transfer (ET) reactions are ubiquitous in physics, chemistry, and biology.[1–3] Long-range ET in chemical and biophysical systems, where the donor (D)–acceptor (A) distance considerably exceeds the spatial extension of both D and of A, is broadly encountered, being central in the context of structural, energetic, electronic, and medium control of ET.[4] Such long-range ET involves the mediation of the nonradiative process by molecular bridges (B), which control the process via multilevel (electronic and/or vibronic) coupling. The nature of bridges for ET in multicenter systems falls into several categories:

(1) Medium bridging. The solvent or the condensed medium spatially intervening between D and A can modify the electronic coupling for ET.[5]

(2) Covalently bound bridges (B) in synthetic DBA supermolecules. ET can be induced by a thermal attachment of a solvated electron e_{solvated} to the donor, i.e., $DBA+e_{\text{solvated}}\rightarrow D^-BA\rightarrow DBA^-$.[6] In a variety of synthetic DBA organic or inorganic molecules ET can be triggered by local electronic-vibrational excitation followed by forward electron transfer and back recombination[7–19] $DBA\xrightarrow{h\nu}D^*BA\rightarrow D^+BA^-\rightarrow DBA$. These ET processes do not involve a D^+B^-A chemical intermediate. A qualitatively different process in some synthetic supermolecules involves the formation of the D^+B^-A chemical intermediate $D^*BA\rightarrow D^+B^-A\rightarrow D^+BA^-$, where DBA is sometimes denoted as DA_1A_2.[20] This mechanism was realized in the porphyrin-quinone (1)–quinone (2) triad [quinone (1)$\equiv$benzoquinone and quinone (2)$\equiv$trichlorobenzoquinone].[20]

(3) Protein bridging in biological systems. These involve multicenter redox metalloenzymes, e.g., blue copper oxidazes,[21,22] cytochrome-*c* oxidazes,[23,24] nitrogenase,[25] and small metalloproteins modified by attachment of electron exchanging groups to particular surface sites, e.g., cytochromes, blue-copper, and other proteins.[26–30]

 0021-9606/97/107(13)/5154/17/$10.00

(4) DNA bridging. DNA doped by Ru^{+2}–Ru^{+3} ions may act as a bridge for ET.[31,32]

(5) Prosthetic groups bridging in membrane proteins.[3,33] In the photosynthetic reaction centers (RCs) of bacteria and green plants the primary process of conversion of solar energy into chemical energy proceeds via a sequence of well organized, highly efficient, directional and specific ET processes between prosthetic groups embedded in the membrane protein medium. In the native bacterial photosynthetic RCs the primary charge separation proceeds via[34,35] $^1P^*BH \rightarrow P^+B^-H \rightarrow P^+BH^-$ (here P, B, and H denote the bacteriochlorophyl dimer, the accessory bacteriochlorophyl, and the bacteriopheophytin, respectively), where B constitutes a bridge for primary ET via a genuine B^- intermediate. Site mutagenesis[36–38] of the RC can either preserve this mechanism for a variety of single-site mutants,[35] while in some other mutants, i.e., tyrosine M 201→tryptophane[39] and the triple-site H bonded mutant[35] an alternative unistep bridging mechanism without the involvement of B^- will be exhibited at low temperatures, i.e., $^1P^*BH \rightarrow P^+BH^-$. Furthermore, chemical modification of the RC, by the substitution of B, can alter the ET mechanism. A dramatic example involves the $B \rightarrow$3-vinyl-13^2-OH-bacteriochlorophyl chemically substituted RC, where the unistep reaction mechanism without involvement of B^- dominates at low temperatures.[40]

(6) Bridging by specific amino acid residues in membrane proteins. A well established case involves the role of the tryptophane M251 residue, which lies close to the quinone (Q) in the bacterial RCs of *R.sphaeroides* and *Rp.viridis* in bridging the quinone unistep reduction process[41] $P^+BH^-(YM251)Q \rightarrow P^+BH(YM251)Q^-$. The Q reduction is dramatically retarded by site mutation of tryptophan by an aliphatic amino acid residue.[41]

The generality of bridging for long-range ET implies that multicenter ET can occur via two limiting mechanisms:

A. Sequential ET

$$\mathrm{DBA} \overset{k_{DB}}{\rightarrow} \mathrm{D^+B^-A} \underset{k_{AB}}{\overset{k_{BA}}{\rightleftarrows}} \mathrm{D^+BA^-}. \tag{1.1}$$

The nonadiabatic coupling inducing sequential ET involves resonance coupling between the relevant (quasidegenerate) vibronic levels of DBA ($\{|\alpha\rangle\}$ manifold with energies E_α) with D^+B^-A and of the vibronic levels of D^+B^-A with D^+BA^- (Fig. 1). Furthermore, the density of vibronic states in the D^+B^-A and D^+BA^- manifolds at energies quasidegenerate with $|\alpha\rangle$ has to be sufficiently large to insure irreversible relaxation. For sequential ET a genuine chemical intermediate, Eq. (1.1), is realized.

B. Superexchange mediated ET

$$\mathrm{DBA} \overset{k_{\mathrm{SUPER}}}{\rightarrow} \mathrm{D^+BA^-}. \tag{1.2}$$

The nonadiabatic coupling inducing superexchange mediated ET[7,42] involves off-resonance coupling between the relevant vibronic levels of DBA and D^+BA^- (Fig. 1), with the density of states in the D^+BA^- manifold quasidegenerate with the doorway state being sufficiently large to insure irreversible relaxation (Fig. 1). For the unistep superexchange mediated ET no chemical intermediate is realized.

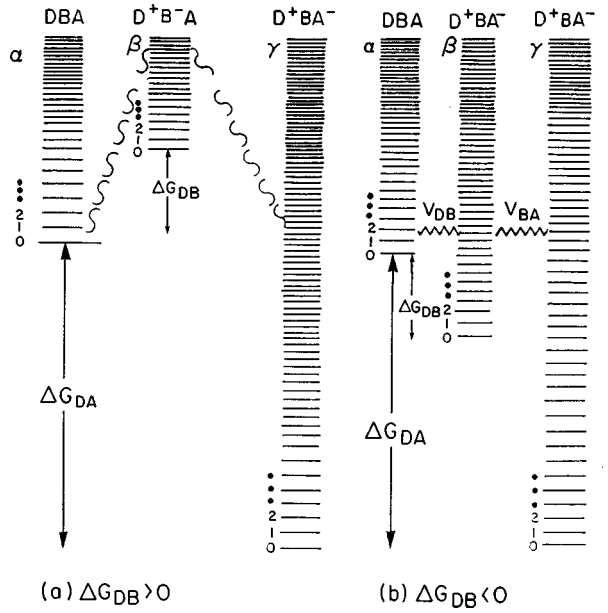

FIG. 1. Vibronic level structure and coupling scheme for ET in a three-electronic state DBA, D^+B^-A, and D^+BA^- system. The doorway states $DBA|\alpha\rangle$ (energies E_α) are in resonance with the final $\{D^+BA^-|\gamma\rangle\}$ quasicontinuum for all E_α. For $\Delta G_{DB}<0$ [case (b)] the coupling of the doorway states $DBA|\alpha\rangle$ with the mediating quasicontinuum $\{D^+B^-A|\beta\rangle\}$ is in resonance (labeled: ''Sequential'') for all E_α. For $\Delta G_{DB}>0$ [case (a)] the $DBA|\alpha\rangle$–$\{D^+B^-A|\beta\rangle\}$ coupling is in off-resonance (labeled: ''Superexchange'').

The basic difference between sequential and superexchange mediated ET involves chemical mediation in the former case and physical mediation in the latter case. Resonance coupling, needed for sequential ET, exists under the condition $\Delta G_{DB}<E_\alpha$, whereas the condition for off-resonance coupling and superexchange ET is $\Delta G_{DB}>E_\alpha$ (where ΔG_{DB} is the energy gap between the electronic origins of D^+B^-A and the DBA manifolds). Obviously, for the coupling and decay of the electronic origin ($|\alpha\rangle=|0\rangle$ and $E_\alpha=0$) of the DBA manifold, the sequential process occurs for $\Delta G_{DB}<0$, while the superexchange process prevails for $\Delta G_{DB}>0$.

The energetic control of the nature of coupling and relaxation is of considerable interest in the context of the optimization of ET and some of its inherent applications, e.g., electron transport through wires in molecular electronics[43] and the mechanism of primary charge separation in photosynthesis.[3,33] On the theoretical front, extensive studies have been performed for the superexchange mechanism ($\Delta G_{DB} \gg 0$) with the electronic interactions being determined by pathway and bond counting (''through-bond'') schemes.[44] Of considerable current interest is the transition from the superexchange to the sequential mechanism, which can be realized by changing the energy gap ΔG_{DB} from

$\Delta G_{DB} \gg 0$ to $\Delta G_{DB} < 0$ (Fig. 1). Kharkats, Kuznetsov, and Ulstrup[45] considered three-level ET addressing dynamically populated intermediate states, nuclear dynamics, and intermediate state vibrational relaxation. Schemes for the treatment of dissipative three-state systems were proposed by Mak *et al.*,[46] Joseph *et al.*,[47] and Todd *et al.*[48] Mukamel and his colleagues[49] considered the interplay between sequential and superexchange ET using a density matrix formalism, with the sequential mechanism proceeding via the population of the diagonal matrix elements, while superexchange involves the off-diagonal matrix elements (electronic coherence contributions). Mukamel *et al.*[49] have drawn an analogy between the superexchange and sequential ET and the transition from (coherent) near-resonance Raman scattering and (incoherent) resonance fluorescence. Subsequently, Sumi and Kakitani[50] have adopted the formalism of Toyozawa *et al.*[51] for resonance Raman scattering to treat ET via a bridge in terms of opposite limits of a single process. They claim that in the case of resonance coupling the sequential process requires rapid (phonon-induced) thermalization in the intermediate D^+B^-A manifold, while the superexchange mechanism is also realized for resonance coupling in the limit of slow medium induced thermalization.[50] These conclusions drastically differ from our distinction between resonance coupling for sequential ET and off-resonance coupling for superexchange mediated ET (Fig. 1) advanced herein. The definitions of the sequential and the superexchange mechanisms are different. We characterize the sequential two-step mechanism as involving a genuine chemical intermediate D^+B^-A vibronic manifold, which is either thermally equilibrated or not, while the superexchange unistep mechanism does not involve the population of the D^+B^-A manifold, with the dynamics being solely determined by the time evolution of the initial DBA and of the final D^+B^-A manifolds. On the other hand, Sumi and Kakitani[50] characterize the sequential mechanism by vibrational equilibration in the mediating D^+B^-A manifold, while their superexchange mechanism is defined in terms of nonthermalization of the D^+B^-A manifold. Thus for resonance DBA–D^+B^-A coupling in the limit of slow phonon thermalization in the D^+B^-A manifold, when the vibrationally excited vibronic states of D^+B^-A are involved in the ET dynamics, Sumi and Kakitani[50] do maintain that the physical situation of superexchange prevails, while our definition encompasses this situation as sequential ET. Our distinction between the sequential and the superexchange mechanisms rests on the experimentally observable population of the mediating D^+B^-A vibronic manifold which can be interrogated in real life.

From the point of view of general methodology, the analogy between the ET dynamics and the second-order optical processes[49,50] is incomplete, as the ''smooth'' radiative coupling interactions are quantitatively different from the nonradiative Franck–Condon coupling between vibronic continua. The nonradiative coupling between the Franck–Condon quasicontinua are weakly correlated,[52] providing the basis for a sequential decay of a single vibronic level, Eq. (1.1), in the limit of resonance coupling. This physical situation of weakly correlated coupling to a quasicontinuum[52] and between quasicontinua is reminiscent of the random coupling models advanced in the theory of interstate and intrastate molecular dynamics[53] and for the loss of intramolecular coherence in high-order multiphoton excitation and dissociation of polyatomic molecules.[54] In the nonradiative random coupling model for the level scheme of Fig. 1(b) (the resonance coupling situation) the sequential kinetic scheme is applicable with the random coupling providing an internal source of dephasing (memory loss) so that extra thermalization processes are not necessary.

The implications of the coupling to the (intramolecular or medium) vibrational quasicontinuum is central for ET and for other condensed phase nonadiabatic dynamics processes and will be analyzed in this paper in the context of sequential ET via bridges. We shall address the following issues:

(1) Exploring the decay dynamics of a single vibronic level in the DBA manifold into two coupled Franck–Condon quasicontinua D^+B^-A and D^+BA^- under resonance and off-resonance coupling conditions.

(2) Establishing the prevalence of the sequential decay for resonance coupling in a three-state Franck–Condon system without invoking thermalization processes in the intermediate state.

(3) Quantifying the microscopic ET rates from a single vibronic level which correspond to sequential and superexchange rates for resonance and for off-resonance coupling, respectively, by the corresponding quantum expressions.

(4) Determining the energetic control of single-level ET. For ET from a single vibronic level, e.g., the electronic origin of the DBA manifold, a change from sequential ET ($\Delta G_{DB} < 0$) to superexchange ET ($\Delta G_{DB} > 0$) will be exhibited with increasing ΔG_{DB}. For small fixed energy gaps (i.e., ΔG_{DB} being comparable to characteristic vibrational frequencies) a transition from a single vibronic level ($E_\alpha < \Delta G_{DB}$) superexchange to a single vibronic level ($E_\alpha > \Delta G_{DB}$) sequential ET will be realized at $E_\alpha \cong \Delta G_{DB}$ (see Fig. 1).

II. ELECTRON TRANSFER DYNAMICS IN A FRANCK–CONDON SYSTEM WITH TWO QUASICONTINUA

We consider the dynamics in the three vibronic manifolds, which correspond to the electronic states DBA($\equiv$D), D^+B^-A($\equiv$B), and D^+BA^-($\equiv$A) (Fig. 1). The DBA manifold of initial doorway states and the two D^+B^-A and D^+BA^- quasicontinua constitutes harmonic vibronic states, which will be referred to as a Franck–Condon system. The interaction between an initial doorway state in the DBA manifold and the D^+B^-A quasicontinuum can be either of resonance ($\Delta G_{DB} < 0$) or of off-resonance ($\Delta G_{DB} > 0$) character. In the case of resonance interaction, the nature of the coupling between the two quasicontinua, which is characterized by weak correlations, will determine the two-step sequential mechanism. On the other hand, for the case of off-resonance coupling, a single-step superexchange mechanism will result. In what follows we shall utilize the theory of

radiationless processes in large molecules and in the condensed phase[55] to explore the ET dynamics in the three electronic states system.

The level structure, coupling, and dynamics of the model system considered herein consists of distinct electronic manifolds, which correspond to three electronic states (Fig. 1): (i) The initial doorway vibronic states $|\alpha\rangle$ in the DBA electronic state (energy E_α), which can be populated by photoselective optical excitation, or can be thermally populated. We shall consider the coupling of a single $|\alpha\rangle$ state to the quasicontinua. (ii) The mediating vibronic quasicontinuum $\{|\beta\rangle\}$ of the D^+B^-A electronic state with energies E_β. The $|\alpha\rangle$–$\{|\beta\rangle\}$ coupling can correspond either to the resonance or to the off-resonance situation. (iii) The final vibronic quasicontinuum $\{|\gamma\rangle\}$ of the D^+BA^- electronic states with energies E_γ. The interquasicontinuum $\{|\beta\rangle\}$–$\{|\gamma\rangle\}$ coupling is substantial, while the $|\alpha\rangle$–$\{|\gamma\rangle\}$ coupling is negligible.

The Hamiltonian of the system is

$$\begin{aligned}\mathbf{H}=&\sum_\alpha |\alpha\rangle E_\alpha\langle\alpha| + \sum_\beta |\beta\rangle(E_\beta+\Delta G_{DB})\langle\beta| \\ &+\sum_\gamma |\gamma\rangle(E_\gamma+\Delta G_{DA})\langle\gamma| \\ &+\left[\sum_\alpha\sum_\beta |\alpha\rangle V_{\alpha\beta}\langle\beta| + cc\right] \\ &+\left[\sum_\beta\sum_\gamma |\beta\rangle V_{\beta\gamma}\langle\gamma| + cc\right],\end{aligned} \tag{2.1}$$

where $V_{\alpha\beta}=\langle\alpha|\mathbf{H}|\beta\rangle$ and $V_{\beta\gamma}=\langle\beta|\mathbf{H}|\gamma\rangle$ are the coupling matrix elements between the vibronic states. Note that in Eq. (2.1) we consider, in principle, the entire system, without decomposition into the ''relevant'' system and a ''bath.''

The zero-order vibronic states are characterized by the doorway states $|\alpha\rangle=\phi_D\chi_\alpha$, and the two quasicontinua states $\{|\beta\rangle\}=\{\phi_B\chi_\beta\}$ and $\{|\gamma\rangle\}=\{\phi_A\chi_\gamma\}$, where ϕ_D, ϕ_B, and ϕ_A denote electronic wave functions of the three states, respectively, while χ_α, χ_β, and χ_γ denote the nuclear wave functions. The coupling terms in Eq. (2.1) are

$$\begin{aligned}V_{\alpha\beta}&=V_{DB}f(\alpha;\beta),\\ V_{\beta\gamma}&=V_{BA}f(\beta;\gamma),\end{aligned} \tag{2.2}$$

where V_{DB} and V_{BA} (with D≡DBA; B≡D^+B^-A; A≡D^+BA^-) denote the electronic couplings (within the framework of the Condon approximation), while $f(\alpha;\beta)$ and $f(\beta;\gamma)$ are the vibrational overlap integrals

$$\begin{aligned}f(\alpha;\beta)&=\langle\chi_\alpha|\chi_\beta\rangle,\\ f(\beta;\gamma)&=\langle\chi_\beta|\chi_\gamma\rangle.\end{aligned} \tag{2.3}$$

We shall now utilize the theory of radiationless transitions in large molecules and in the condensed phase to explore ET dynamics in this three-electronic states system. As is common in quantum mechanical treatments of kinetic schemes[54,55] the initial condition is taken to be a single (nonstationary) doorway state, i.e., $\Psi(0)=|\overline{\alpha\rangle}$, which will be expressed in terms of a wave packet of molecular eigenstates $\{|j\rangle\}$ of the Hamiltonian. The time evolution of the wave packet of molecular eigenstates contains the relevant information about the time-dependent population probabilities of the doorway state and of the two distinct quasicontinua.

In what follows we explicitly consider the entire level structure of the system. The molecular eigenstates are given by

$$|j\rangle=\sum_\alpha a_\alpha^{(j)}|\alpha\rangle+\sum_\beta b_\beta^{(j)}|\beta\rangle+\sum_\gamma c_\gamma^{(j)}|\gamma\rangle. \tag{2.4}$$

The coefficients in Eq. (2.4) provide the unitary transformation $\underset{\approx}{U}\underset{\approx}{H}\underset{\approx}{U}^+=\underset{\approx}{E}$, which diagonalizes the Hamiltonian, Eq. (2.1), where $U_{j\alpha}=a_\alpha^{(j)}$, $U_{j\beta}=b_\beta^{(j)}$, and $U_{j\gamma}=c_\gamma^{(j)}$. The energies E_j of the molecular eigenstates constitute the diagonal matrix elements of $\underset{\approx}{E}$. The zero-order vibronic states can be reconstructed from the molecular eigenstates

$$\begin{aligned}&|m\rangle=\sum_j (U^+)_{mj}|j\rangle\\ &((U^+)_{mj}=a_\alpha^{(j)}\quad\text{for } m=\alpha,\quad (U^+)_{mj}=b_\beta^{(j)}\quad\text{for } m=\beta,\\ &\text{and } (U^+)_{mj}=c_\gamma^{(j)}\quad\text{for } m=\gamma).\end{aligned} \tag{2.5}$$

The initial state of the system $\Psi(0)=|\overline{\alpha\rangle}$ is expressed in the form

$$\Psi(0)=\sum_j a_\alpha^{(j)}|j\rangle. \tag{2.6}$$

Equation (2.6) provides a wave packet of molecular eigenstates,[55] whose time evolution is

$$\Psi(t)=\sum_j a_\alpha^{(j)}|j\rangle\exp(-iE_jt/\hbar). \tag{2.7}$$

We can now use Eq. (2.7) to obtain explicit expressions for the population probabilities. The population probabilities $P_D(t)$, $P_B(t)$, and $P_A(t)$ of the reactant DBA states, of the mediating D^+B^-A quasicontinuum and of the final D^+BA^- quasicontinuum, respectively, are given by

$$\begin{aligned}P_D(t)&=\sum_\alpha |\langle\alpha|\Psi(t)\rangle|^2=\sum_\alpha\left|\sum_j a_\alpha^{(j)}(t)a_\alpha^{(j)}\right.\\ &\qquad\left.\times\exp(-iE_jt/\hbar)\right|^2,\\ P_B(t)&=\sum_\beta |\langle\beta|\Psi(t)\rangle|^2=\sum_\beta\left|\sum_j a_\alpha^{(j)}(t)b_\beta^{(j)}\right.\\ &\qquad\left.\times\exp(-iE_jt/\hbar)\right|^2,\\ P_A(t)&=\sum_\gamma |\langle\gamma|\Psi(t)\rangle|^2=\sum_\gamma\left|\sum_j a_\alpha^{(j)}(t)c_\gamma^{(j)}\right.\\ &\qquad\left.\times\exp(-iE_jt/\hbar)\right|^2.\end{aligned} \tag{2.8}$$

We now proceed to characterize the initial manifolds $\{|\alpha\rangle\}$ and the two quasicontinua $\{|\beta\rangle\}$ and $\{|\gamma\rangle\}$, as well as the couplings $V_{\alpha\beta}$ and $V_{\beta\gamma}$, Eq. (2.2), within the framework of the harmonic model.

The Franck–Condon system is characterized by the doorway states $\{|\alpha\rangle\}$ of a harmonic potential surface $U_D(q)$, coupled to the mediating $\{|\beta\rangle\}$ states of the potential surface $U_B(q)$, which are in turn coupled to the final states $\{|\gamma\rangle\}$ of the potential surface $U_A(q)$. The level structure and the couplings will be described by the three multidimensional displaced nuclear potential surfaces $U_D(q)$, $U_B(q)$, and $U_A(q)$, which are characterized by the same frequencies. The relevant n vibrational modes are characterized by the coordinates $\mathbf{q}\equiv\{q_1,q_2,\ldots,q_n\}$, masses $\mathbf{m}=\{m_1,m_2,\ldots,m_n\}$, and frequencies $\boldsymbol{\omega}=(\omega_1,\omega_2,\ldots,\omega_n\}$. The displacements of the equilibrium positions between the minima of the potential surfaces $I=$D or B and $J=$B or A are $\Delta q_{IJ}\equiv\{\Delta q_1^{IJ},\Delta q_2^{IJ},\ldots,\Delta q_n^{IJ}\}$. It will be useful to define the reduced displacements $\Delta^{IJ}=\{\Delta_1^{IJ},\Delta_2^{IJ},\ldots,\Delta_n^{IJ}\}$, where $\Delta_k^{IJ}=\Delta q_k^{IJ}/(2\hbar/\omega_k m_k)^{1/2}$. The reorganization energy between the I and J states is

$$\lambda_{IJ}=\mathbf{S}^{IJ}\cdot\omega, \tag{2.9}$$

where $\mathbf{S}^{IJ}=\{S_1^{IJ},S_2^{IJ},\ldots,S_n^{IJ}\}$ and $S_k^{IJ}=|\Delta_k^{IJ}|^2$. The energy gaps between the minima of the potential surfaces $U_I(q)$ and $U_J(q)$ are denoted by ΔG_{IJ}. The three classes of vibronic states will be specified in terms of the occupation numbers of the vibrational modes, i.e., $|\alpha\rangle\equiv\{\alpha_1,\alpha_2,\alpha_3,\ldots,\alpha_n\}$, $|\beta\rangle\equiv\{\beta_1,\beta_2,\ldots,\beta_n\}$, and $|\gamma\rangle\equiv\{\gamma_1,\gamma_2,\ldots,\gamma_n\}$. The single-mode vibrational overlap between the i_k state ($i=\alpha$ or β) and the final f_k state ($f=\beta$ or γ) of the mode k is

$$f(i_k;f_k)=\exp(-\Delta^2/2)(i!f!)\times\sum_{r=0}^{\min(i,f)}\frac{(-1)^{i+f-r}\Delta^{i+f-2r}}{r!(i-r)!(f-r)!}, \tag{2.10}$$

where on the rhs of Eq. (2.10) we abbreviate $\Delta=\Delta_k$, $i=i_k$, and $f=f_k$. The Franck–Condon vibrational overlap integrals, Eq. (2.3), are

$$f(\alpha;\beta)=\prod_{k=1}^{n}f(\alpha_k;\beta_k),\qquad f(\beta;\gamma)=\prod_{k=1}^{n}f(\beta_k;\gamma_k). \tag{2.11}$$

Finally, we have to specify the magnitudes of the electronic coupling terms V_{DB} and V_{BA}. Equation (2.8), together with Eqs. (2.1), (2.2), (2.10), and (2.11), provides the entire information on the coupling and dynamics.

Of some interest are the scaling properties and the energetic and dynamic attributes. We introduce a scaling parameter σ. Keeping the reduced displacements Δ^{IJ} fixed, the scaled parameters $\sigma\omega$, $\sigma\lambda_{IJ}$, $\sigma\Delta E_{IJ}$, and σV_{IJ} will yield invariant results for the spectral density. With these scaled parameters the time scales as t/σ.

III. COUPLINGS, CORRELATIONS, AND SPECTRAL DENSITIES

We have performed numerical model calculations for the level structure, coupling, and dynamics in a four-mode harmonic model with $\omega/\mathrm{cm}^{-1}=\{117\ \ 75\ \ 35\ \ 27\}$ of the three displaced potential surfaces. For the vibronic coupling between the mediating and the final state we took $S_{BA}=\{1.1\ \ 2\ \ 3\ \ 3\}$ and $\Delta_{BA}=\{1.05\ \ 1.41\ \ 1.73\ \ 1.73\}$, the corresponding value of the reorganization energy, Eq. (2.9), is $\lambda_{BA}=\mathbf{S}_{BA}\omega^{+}=464.7\ \mathrm{cm}^{-1}$. The relation between the reorganization energy λ_{BA} and the other two reorganization energies was chosen as $\lambda_{BA}=\lambda_{DB}$ and $\lambda_{DA}=2\lambda_{DB}$. This choice of parameters allows for a nonunique choice of the reduced displacement vectors Δ_{DB} and Δ_{BA}. Constructing a vector $\mathbf{D}_{IJ}$ with the components $\Delta_k^{IJ}(\omega_k)^{1/2}$ we have $\lambda_{IJ}=\mathbf{D}_{IJ}\mathbf{D}_{IJ}^{+}$ ($I=$D or B; $J=$A or B) and $\lambda_{DA}=(\mathbf{D}_{DB}-\mathbf{D}_{BA})\cdot(\mathbf{D}_{DB}-\mathbf{D}_{BA})^{+}$. Equation (2.9) then results in the two equations $\mathbf{D}_{DB}\mathbf{D}_{BA}^{+}=0$ and $\lambda_{BA}=\lambda_{DB}=\mathbf{D}_{DB}\cdot\mathbf{D}_{DB}^{+}$. As λ_{BA} and $\mathbf{D}_{BA}$ were fixed, the vector $\mathbf{D}_{DB}$ was found by taking (arbitrarily) two of its elements and then obtaining the other two elements from the solution of the two equations given above. Such a solution is $\Delta_{DA}=\{-0.88\ \ 1.49\ \ -2.03\ \ 1.54\}$. The reorganization energies are $\lambda_{DB}=\lambda_{BA}=464.7\ \mathrm{cm}^{-1}$ and $\lambda_{DA}=929.4\ \mathrm{cm}^{-1}$.

The initial doorway state is in most cases the ground vibrational state ($|\overline{\alpha}\rangle=|0\rangle$) of DBA located at $E_0=0$. The $\{|\alpha\rangle|\}$ doorway manifold is taken to contain $n_\alpha=1-50$ state(s). The electronic origin of the final $\{|\gamma\rangle\}$ manifold is characterized by $\Delta G_{DA}=-450\ \mathrm{cm}^{-1}$ and it contains $n_\gamma=1000-2000$ states (up to excess vibrational energy in the D^+BA^- manifold of $545-671\ \mathrm{cm}^{-1}$, i.e., $95-221\ \mathrm{cm}^{-1}$ above the electronic origin ($|\overline{\alpha}\rangle=|0\rangle$) of the doorway state). The mediating vibronic manifold $\{|\beta\rangle\}$ is characterized by the energy gap ΔG_{DB} (which will be varied in the range $\Delta G_{DB}=-450-450\ \mathrm{cm}^{-1}$) and it includes $n_\beta=1000-2000$ vibronic states (up to excess vibrational energy in the D^+B^-A manifold of $671\ \mathrm{cm}^{-1}$, i.e., $221\ \mathrm{cm}^{-1}$ above the electronic origin of the ($|\overline{\alpha}\rangle=|0\rangle$) doorway state). The vibronic couplings were calculated from Eqs. (2.2), (2.3), (2.10), and (2.11). Making contact with the conventional classification of couplings in ET (although we note that in the present case we consider single-state dynamics involving nuclear tunneling from the doorway state) the following situations are of interest. (1) Resonance DBA–D^+B^-A coupling ($\Delta G_{DB}=-450\ \mathrm{cm}^{-1}$ to 0). In this case $-\Delta G_{DB}\leqslant\lambda_{DB}$, so that the DBA–$\{D^+B^-A\}$ dynamics corresponds to a transition from the activationless situation ($-\Delta G_{DB}\cong\lambda_{DB}$) to the normal ET region. (2) Off-resonance DBA–D^+B^-A coupling ($\Delta G_{DB}=0-450\ \mathrm{cm}^{-1}$). This is the case of the mediated DBA–$\{D^+BA^-\}$ dynamics, and as $-\Delta G_{DA}<\lambda_{DA}$ it corresponds to the ''normal'' ET situation. Finally, the electronic couplings were taken as $V_{DB}=35\ \mathrm{cm}^{-1}$ and $V_{BA}=25\ \mathrm{cm}^{-1}$ for the DBA–D^+B^-A resonance coupling and $V_{BD}=100-200\ \mathrm{cm}^{-1}$ and $V_{BA}=200-300\ \mathrm{cm}^{-1}$ for the off-resonance case. These electronic couplings were chosen to give ET dynamics on the ultrafast time scale 300–4000 fs. The choice of the energy parameters was guided by the fol-

lowing considerations: (1) The attainment of vibrational quasicontinua, i.e., $\Delta G_{IJ} \gg \omega_i$ for all vibrational frequencies. (2) The realization of the strong coupling situation, i.e., $\langle V^2_{\alpha\beta}\rangle^{1/2}\rho_\beta > 1$, $\langle V^2_{\beta\gamma}\rangle^{1/2}\rho_\gamma > 1$ for the resonance coupling and

$$\left\langle \left(\frac{V_{\alpha\beta}V_{\beta\gamma}}{\Delta E} \right)^2 \right\rangle^{1/2} \rho_\gamma > 1$$

for the off-resonance interactions. Here ρ_β and ρ_γ are the densities of states of the $\{|\beta\rangle\}$ and $\{|\gamma\rangle\}$ manifolds, while ΔE is a mean energy denominator for superexchange interactions. Under these circumstances the statistical limit for intramolecular or condensed phase dynamics is realized with time scales $t \sim \hbar[2\pi\langle V^2_{\alpha\beta}\rangle\rho_\beta]^{-1}$ for resonance coupling. (3) Negligible edge effects for the coupling of the doorway state to a quasicontinuum or for the coupling between the quasicontinua. This extensive input information will now be utilized to explore the characteristics of the couplings within the three-electronic states system.

An important feature of the coupling between the initial manifold $\{|\alpha\rangle\}$ with the $\{|\beta\rangle\}$ quasicontinuum and of the $\{|\beta\rangle\}$–$\{|\gamma\rangle\}$ interquasicontinua coupling involves the correlations $\eta_{\alpha\alpha'}$ (for different $|\alpha\rangle$ and $|\alpha'\rangle$) or $\eta_{\beta\beta'}$ (for distinct $|\beta\rangle$ and $|\beta'\rangle$ states), which are quantified by

$$\begin{aligned} \eta_{\alpha\alpha'} &= \langle V_{\alpha\beta}V_{\beta\alpha'}\rangle / [\langle V^2_{\alpha\beta}\rangle\langle V^2_{\beta\alpha'}\rangle]^{1/2}, \\ \eta_{\beta\beta'} &= \langle V_{\beta\gamma}V_{\gamma\beta'}\rangle / [\langle V^2_{\beta\gamma}\rangle\langle V^2_{\gamma\beta'}\rangle]^{1/2}, \end{aligned} \tag{3.1}$$

where $\langle\ \rangle$ denotes the average over the energy range δE, where the density of states is ρ, i.e.,

$$\begin{aligned} &\langle V_{\alpha\beta}V_{\beta\alpha'}\rangle = (\rho_\beta \delta E)^{-1} \sum_\beta V_{\alpha\beta}V_{\beta\alpha'}, \\ &E_\alpha, E_{\alpha'} \in \delta E. \end{aligned} \tag{3.2}$$

The energy range δE has to span the relevant $\{|\beta\rangle\}$ states which contribute to interference between $|\alpha\rangle$ and $|\alpha'\rangle$.[56,57] An expression analogous to Eq. (3.2) is given for $\langle V_{\beta\gamma}V_{\gamma\beta'}\rangle$. Numerical calculations were performed for $\eta_{\alpha\alpha'}$ with α and α' in the vicinity of the electronic origin of DBA, i.e., for $\alpha,\alpha' = 1$–40 (where $\alpha = 1$ denoted the electronic origin). Concurrently, numerical calculations of $\eta_{\beta\beta'}$ for the $\{|\beta\rangle\}$–$\{|\gamma\rangle\}$ interquasicontinua coupling were performed in the vicinity of the doorway state, i.e., $\beta,\beta' = 150$–190. The correlation parameters $|\eta_{\alpha\alpha'}|$ for the pairs α and α' of doorway states in the vicinity of the electronic origin of the DBA manifold [Fig. 2(a)] are considerably lower than unity, with the highest values of the correlation parameters falling in the range $|\eta_{\alpha\alpha'}| = 0.5$–0.2. The small number of relatively high values of $|\eta_{\alpha\alpha'}|$ corresponds to members of a vibrational progression with α and α' differing only by a single vibrational quantum number, while for multimode changes between α and α' very low values of $|\eta_{\alpha\alpha'}|$ are exhibited.[52(a)] The propensity rules[52(b)] for coupling to a Franck–Condon quasicontinuum imply the existence of weak, but finite, correlations $|\eta_{\alpha\alpha'}|$ for the $\{|\alpha\rangle\}$–$\{|\beta\rangle\}$ coupling in the vicinity of the electronic origin of the doorway states manifold $\{|\alpha\rangle\}$. In this low-energy domain the level structure in the $\{|\alpha\rangle\}$ manifold is sparse, i.e., the nonradiative widths of the resonances are small relative to their spacing. Accordingly, interference effects in the nonradiative decay of a single $|\alpha\rangle$ doorway state will be negligible and $P_D(t)$, Eq. (2.8), is expected to be well described in terms of the golden rule. The situation is qualitatively similar for the interquasicontinua $\{|\beta\rangle\}$–$\{|\gamma\rangle\}$ coupling. The correlation parameters $\eta_{\beta\beta'}$ [Fig. 2(b)] are lower, i.e., $|\eta_{\beta\beta'}| \leqslant 0.2$–0.3, in accord with the propensity

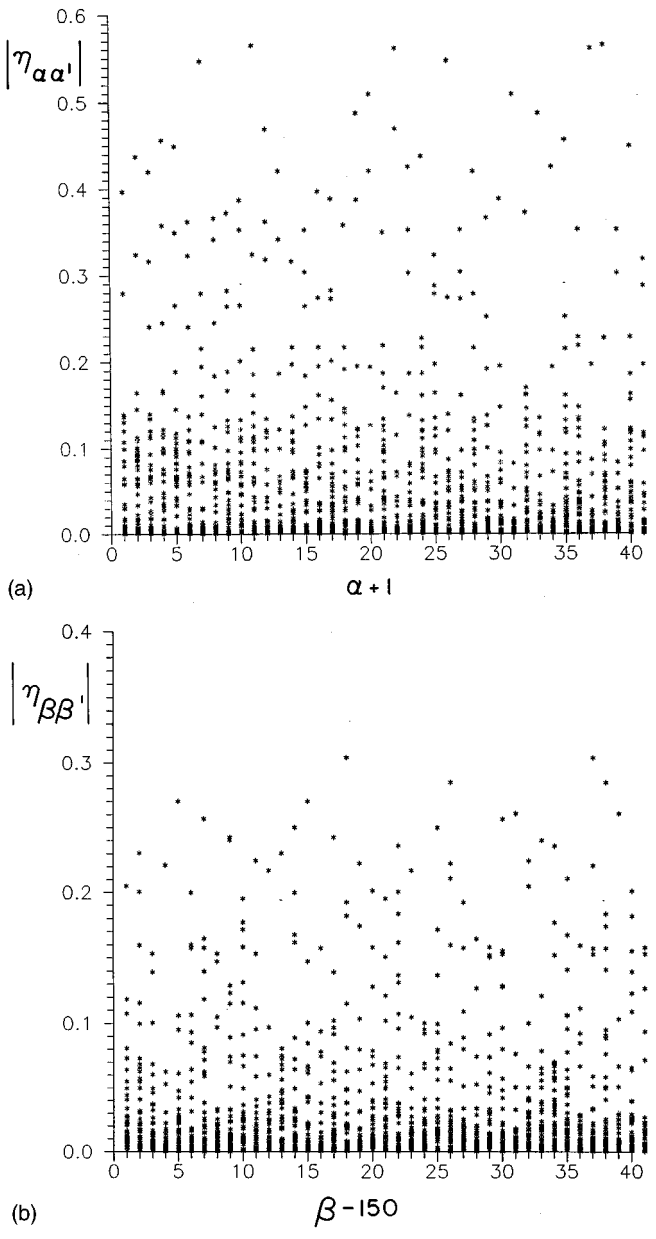

FIG. 2. Absolute values of the correlation parameters $|\eta_{\alpha\alpha'}|$ and $|\eta_{\beta\beta'}|$ between the doorway states α,α' and between the quasicontinuum states β,β'. Data for a four-mode Franck–Condon system (Sec. III) with the coupling parameters $\lambda_{DB} = 460\ \mathrm{cm}^{-1}$ and $\lambda_{BA} = 465\ \mathrm{cm}^{-1}$. The energy gaps are $\Delta G_{DB} = -300$ and $\Delta G_{DA} = -600\ \mathrm{cm}^{-1}$. (a) $|\eta_{\alpha\alpha'}|$. The energy range is $200\ \mathrm{cm}^{-1} \leqslant E_\beta \leqslant 550\ \mathrm{cm}^{-1}$, containing $N = 40$ states (in the range $\alpha = 1$–40) and 1560 values of $|\eta_{\alpha\alpha'}|$. The electronic origin of the $\{|\alpha\rangle\}$ manifold is denoted as $|\alpha\rangle = |0\rangle$. (b) $|\eta_{\beta\beta'}|$. The energy range is $500\ \mathrm{cm}^{-1} \leqslant E_\gamma \leqslant 700\ \mathrm{cm}^{-1}$, containing $N = 40$ states (in the range $\beta = 150$–190) and 1560 values of $|\eta_{\beta\beta'}|$.

rules. These small $|\eta_{\beta\beta'}|$ correlations imply that the inter-quasicontinua $\{|\beta\rangle\}$–$\{|\gamma\rangle\}$ couplings approach the random coupling situation (i.e., $\eta_{\beta\beta'}=0$ for all β, β').[54] The dynamic implications of this nearly random coupling are of considerable importance implying the occurrance of sequential time evolution.

To characterize the coupling in the Franck–Condon quasicontinuum we consider first the $|\alpha\rangle$–$\{|\beta\rangle\}$ coupling for different doorway states. The Franck–Condon density for an individual $|\alpha\rangle$ state is

$$\mathrm{FD}(\alpha)=\sum_{\beta}|f(\alpha;\beta)|^2\delta(E_\alpha-E_\beta), \tag{3.3}$$

where $|f(\alpha;\beta)|^2$ are the Franck–Condon factors, expressed in terms of the vibrational overlap integrals, Eq. (2.11). For coupling to the $\{|\beta\rangle\}$ quasicontinuum $\mathrm{FD}(\alpha)$ is expressed in the form

$$\mathrm{FD}(\alpha)=(\delta E)^{-1}\sum_{\{\beta\}}|f(\alpha;\beta)|^2, \tag{3.4}$$

where the discrete sum is taken over the states $\{\beta\}$ within an energy range δE around the energy of the doorway state $|\alpha\rangle$. In what follows we shall present some numerical data for the Franck–Condon densities $\mathrm{FD}(\alpha)$, Eq. (3.4), for the lower doorway state $\alpha=0$, coarse grained over δE. For the lowest doorway state $\alpha=0$ (Fig. 3), the density FD(0) is Poissonian of the form $\exp(-\lambda)\lambda^n/n!$ where $n\cong E_v/\hbar\langle\omega\rangle$, with E_v being the excess vibrational frequency. The FD(0) distribution peaks at $E_v\cong\lambda_{DB}=430\ \mathrm{cm}^{-1}$, while for higher $|\alpha\rangle$ states the spread of $\mathrm{FD}(\alpha)$ occurs over a larger E_v range. The Franck–Condon densities $\mathrm{FD}(\beta)$ for individual $|\beta\rangle$ states for the $\{|\beta\rangle\}$–$\{|\gamma\rangle\}$ coupling exhibit a spread over a broad E_v domain, reflecting the features of the intercontinua coupling. In view of the small correlation parameters $\eta_{\beta\beta'}$ for the $\{|\beta\rangle\}$–$\{|\gamma\rangle\}$ coupling [Fig. 2(b)] these (diagonal) spectral densities are expected to dominate the intercontinuum dynamics.

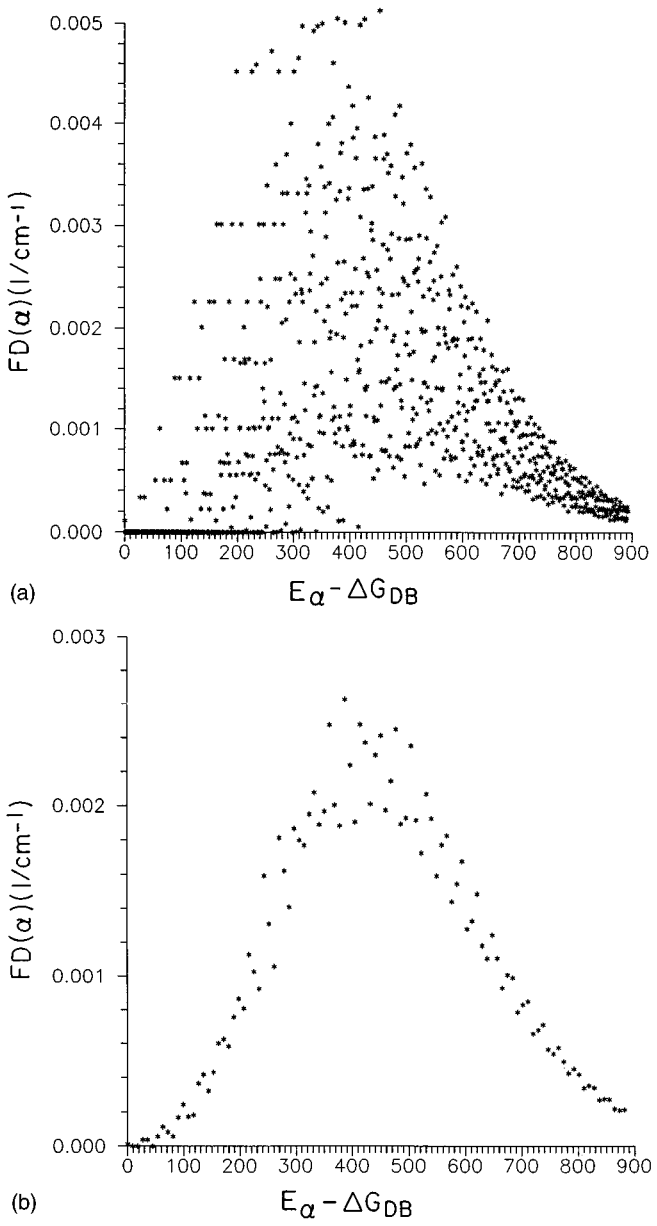

FIG. 3. Spectral densities $\mathrm{FD}(\alpha)$, Eq. (3.4), for the lowest doorway state $|\alpha\rangle$ (i.e., the electronic origin of DBA). (a) Energy averaging over 1 cm^{-1}. (b) Energy averaging over 9 cm^{-1}.

IV. MODEL SIMULATIONS FOR ET DYNAMICS

We shall now proceed to explore the dynamics in the three electronic states DBA, $\mathrm{D^+B^-A}$, and $\mathrm{D^+BA^-}$ system, describing the potential surfaces in terms of a four-mode harmonic model advanced in Sec. III. The molecular eigenstates $\{|j\rangle\}$, Eq. (2.4), their energies $\{E_j\}$ and the coefficients $\{a_\alpha^{(j)}\}$, $\{b_\beta^{(j)}\}$, and $\{c_\gamma^{(j)}\}$ of the transformation matrix U, Eq. (2.5), were obtained by the diagonalization of the $(n_\alpha+n_\beta+n_\gamma)\times(n_\alpha+n_\beta+n_\gamma)$ dimensional Hamiltonian, Eq. (2.1). To make contact with realistic experimental conditions the ''propagation'' of the initial doorway state $|\overline{\alpha}\rangle$, Eq. (1.6), has to be modified. The unrestricted summation over the molecular eigenstates in Eq. (2.6) was replaced by a sum over a restricted energy range $\delta E\cong 50\ \mathrm{cm}^{-1}$ of the order of the spectral width of a short excitation pulse. Subsequently, the time dependence of the population probabilities, Eq. (2.8), was calculated. The input parameters for the simulations were presented in Sec. III. The results of the quantum-mechanical simulations will now be presented for the limits of resonance ($\Delta G_{DB}<0$) and off-resonance ($\Delta G_{DB}>0$) coupling.

A. Resonance DBA–$\mathrm{D^+B^-A}$ coupling ($\Delta G_{DB}<0$)

We consider the decay of a single doorway state, which corresponds to the electronic origin $|\alpha\rangle=|0\rangle$ of the DBA manifold, into the two coupled $\mathrm{D^+B^-A}$ and $\mathrm{D^+BA^-}$ quasicontinua. As the density of states in the DBA manifold in the vicinity of the doorway state is low, we disregard the reverse process $\mathrm{D^+B^-A}\rightarrow\mathrm{DBA}$ in the kinetic scheme (1.1). Figure 4 presents the time dependence of the population probabilities $P_D(t)$, $P_B(t)$, and $P_A(t)$, Eq. (2.8), simulated for the energy range $\Delta G_{DB}=-450--150\ \mathrm{cm}^{-1}$. The population probability $P_D(t)$ of the doorway state decreases exponentially,

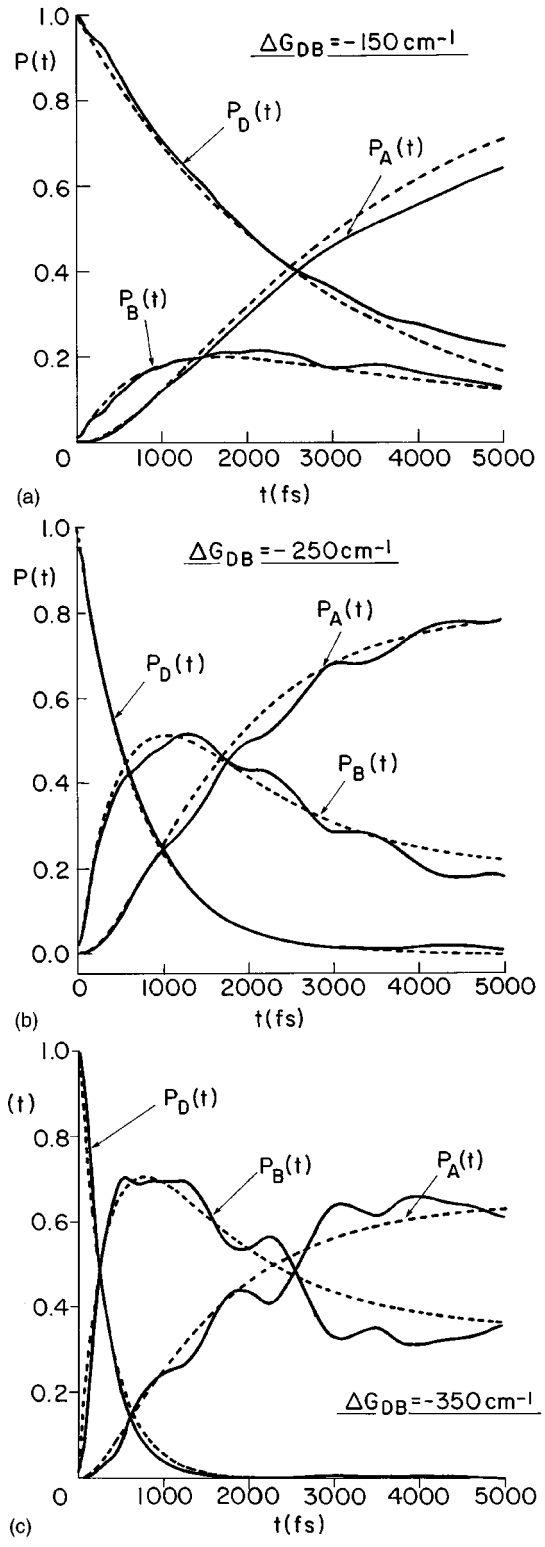

FIG. 4. Quantum-mechanical simulations of sequential ET. Time dependence of the population probabilities $P_D(t)$, $P_B(t)$, and $P_A(t)$, Eq. (2.8), for $\Delta G_{DB}<0$. Decay from the initial $|\alpha\rangle=|0\rangle$ doorway state. The solid curves represent the results of the simulation. The dashed curves represent the kinetic fit, Eq. (4.1), of the simulated curves with the sequential rates k_{DB}, k_{BA}, and k_{AB} summarized in Fig. 5. Simulations for a four-mode system (Sec. III). Electronic couplings $V_{DB}=35\ \mathrm{cm}^{-1}$, $V_{BA}=25\ \mathrm{cm}^{-1}$ and nuclear couplings $\lambda_{DB}=465\ \mathrm{cm}^{-1}$ and $\lambda_{BA}=930\ \mathrm{cm}^{-1}$ with displacement vectors Δ specified in Sec. III. (a) $\Delta G_{DB}=-150\ \mathrm{cm}^{-1}$. (b) $\Delta G_{DB}=-250\ \mathrm{cm}^{-1}$. (c) $\Delta G_{DB}=-350\ \mathrm{cm}^{-1}$.

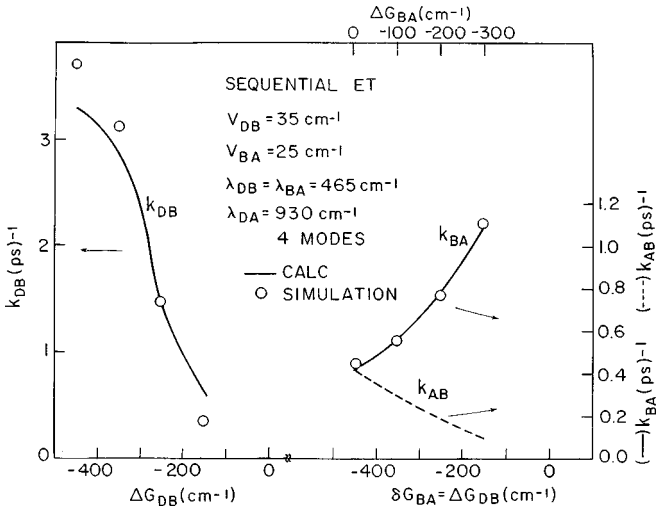

FIG. 5. The energy-gap (ΔG_{DB}) dependence of the sequential ET rates k_{DB}, k_{BA}, and k_{AB} from the electronic origin of DBA obtained from the kinetic fit of the simulated $P_D(t)$, $P_B(t)$, and $P_A(t)$ curves (Fig. 4). Four-mode system (Sec. III) electronic and nuclear couplings are marked on the figure. The simulated rates (○) are compared with the calculated (—) quantum mechanical rates, Eqs. (5.1), (5.2), and (5.8).

while the population probability for the buildup of the final D^+BA^- quasicontinuum exhibits at short times a $P_A(t) \propto t^2$ dependence, as appropriate for sequential kinetics. Most important, the population probability $P_B(t)$ of the mediating D^+B^-A quasicontinuum exhibits a rise and fall towards a long-time saturation, as appropriate for a genuine chemical intermediate. The fluctuations in the simulated probabilities reflect the features of the finite system used herein. These population probabilities can be well described by a consecutive kinetic scheme, Eq. (1.1), with the conventional kinetic equations

$$P_D(t)=\exp(-k_{DB}t), \tag{4.1a}$$
$$P_B(t)=a_1+a_2\ \exp(-k_{DB}t)+a_3\ \exp[-(k_{BA}+k_{AB})t]$$

with

$$a_1=\frac{k_{AB}}{k_{BA}+k_{AB}};\quad a_2=\frac{k_{DB}-k_{AB}}{k_{BA}+k_{AB}-k_{DB}}, \tag{4.1b}$$
$$a_3=\frac{k_{DB}k_{BA}}{(k_{DB}-k_{BA}-k_{AB})(k_{BA}+k_{AB})},$$

and

$$P_A(t)=1-P_D(t)-P_B(t). \tag{4.1c}$$

The analysis of the dynamic data over a broad range of ΔG_{DB} provided the rate constants k_{DB}, k_{BA} and k_{AB} for the sequential kinetic scheme (1.1), which are presented vs ΔG_{DB} in Fig. 5. No systematic deviations from the kinetic scheme, Eqs. (1.1) and (4.1) were observed. From these results we conclude that:

(1) The resonance doorway state $|\alpha\rangle$—quasicontinuum $\{|\beta\rangle\}$ coupling, in conjunction with resonance coupling between the two $\{|\beta\rangle\}$ and $\{|\gamma\rangle\}$ Franck–Condon quasicontinua, results in a sequential chemical kinetics.

(2) The sequential kinetics for the $|\alpha\rangle$–$\{|\beta\rangle\}$–$\{|\gamma\rangle\}$ system reflects the implications of the nearly random resonance coupling between the Franck–Condon quasicontinua. It is known that in a random coupled $|\alpha\rangle$–$\{|\beta\rangle\}$–$\{|\gamma\rangle\}$ system (with $\eta_{\alpha\alpha'}=0$ and $\eta_{\beta\beta'}=0$) sequential kinetics prevails.[54] Our analysis establishes that the coupling between Franck–Condon quasicontinua is close to random and gives sequential kinetics.

(3) Making contact with experimental reality we demonstrate that sequential kinetics prevails in the three electronic states DBA–D^+B^-A–D^+BA^- system, which satisfies two conditions: (i) DBA–D^+B^-A ($|\alpha\rangle$–$\{|\beta\rangle\}$) resonance coupling and (ii) sufficiently high densities of states in the $\{|\beta\rangle\}$ and $\{|\gamma\rangle\}$ quasicontinua to insure nonradiative dynamics in the statistical limit. In particular, the time-dependent population probability of the intermediate D^+B^-A quasicontinuum reflects the chemical mediation via a bridge.[3,20,33–35]

(4) Our simulations demonstrate that in the DBA–D^+B^-A–D^+BA^- system with DBA–D^+B^-A resonance coupling sequential kinetics occurs even in the absence of vibrational relaxation in the mediating D^+B^-A manifold. This conclusion is in contrast with the analysis of Sumi and Kakitani,[50] which rests on a different definition of the sequential mechanism, and which implies that for resonance coupling sequential ET is necessarily induced by rapid phonon-induced thermalization in the intermediate D^+B^-A manifold. Our simulations reveal that for resonance DBA$|\alpha\rangle$–$D^+B^-A\{|\beta\rangle\}$ coupling the weakly correlated coupling between the Franck–Condon ''bumpy'' quasicontinua provides a phase erosion mechanism for the dynamics, resulting in the population of the D^+B^-A manifold, i.e., sequential kinetics without the need of intermediate dephasing processes.

Our simulations for the resonance $|\alpha\rangle$–$\{|\beta\rangle\}$ coupling situation, which result in sequential kinetics (Fig. 4), were conducted for the region $\Delta G_{DB} \leqslant -150\ \mathrm{cm}^{-1}$. For lower absolute values of the (negative) ΔG_{DB} energy gap, the density of states in the D^+B^-A $\{|\beta\rangle\}$ manifold is too low in our four-mode system, so that the conditions for irreversible decay in the statistical limit (Sec. III) are violated. This difficulty stems from the intrinsic limitations of the four-mode system used herein. The number of vibrational modes is limited by the size (3000×3000) Hamiltonian matrix used in our simulations. For realistic condensed phase or molecular systems, where the number of vibrational degrees of freedom will be considerably higher and where low-frequency vibrational modes contribute, the irreversible (sequential) dynamics will prevail for higher values of ΔG_{DB} (<0).

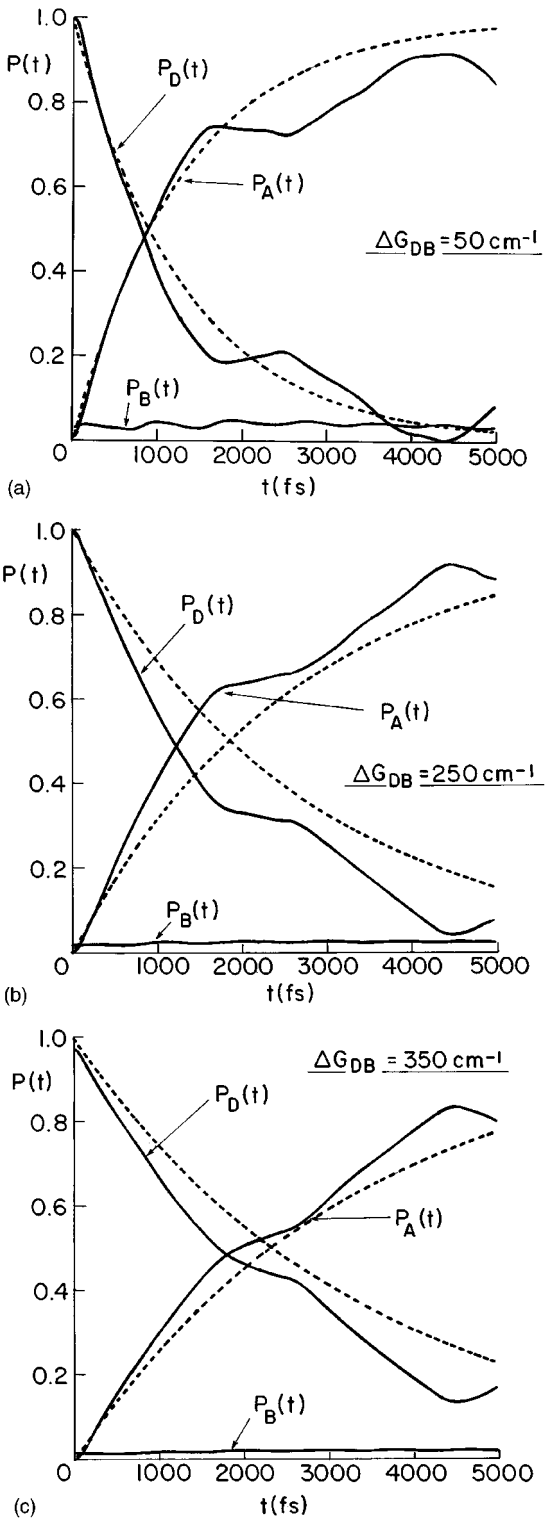

FIG. 6. Quantum-mechanical simulations of superexchange ET. Time dependence of the population probabilities $P_A(t)$, $P_B(t)$, and $P_D(t)$, Eq. (2.8), for $\Delta G_{DB}>0$, with decay from the initial $|\alpha\rangle=|0\rangle$ doorway state. Simulations for a four-mode system (Sec. III). Electronic couplings $V_{DB}=100\ \mathrm{cm}^{-1}$ and $V_{BA}=250\ \mathrm{cm}^{-1}$ and nuclear couplings $\lambda_{DB}=465\ \mathrm{cm}^{-1}$ and $\lambda_{BD}=930\ \mathrm{cm}^{-1}$, with displacement vectors Δ specified in Sec. III. The solid curves represent the results of the simulations. The dashed curves represent the kinetic fit, Eq. (4.2), of the simulated $P_D(t)$ and $P_A(t)$ curves, with the superexchange rate k_{SUPER} summarized in Fig. 7. (a) $\Delta G_{DB}=50\ \mathrm{cm}^{-1}$. (b) $\Delta G_{DB}=250\ \mathrm{cm}^{-1}$. (c) $\Delta G_{DB}=350\ \mathrm{cm}^{-1}$.

B. Off-resonance DBA–D^+B^-A coupling ($\Delta G_{DB}>0$)

We now consider the coupling of the single doorway state $|\alpha\rangle=|0\rangle$ in the DBA manifold with the final $D^+BA^-\{|\gamma\rangle\}$ quasicontinuum, which is mediated by off-resonance superexchange $|\alpha\rangle$–$\{|\gamma\rangle\}$ coupling with the DBA manifold. The direct $|\alpha\rangle$–$\{|\gamma\rangle\}$ coupling is considered to be negligible. Figure 6 presents the time dependence of the population probabilities simulated for the energy range

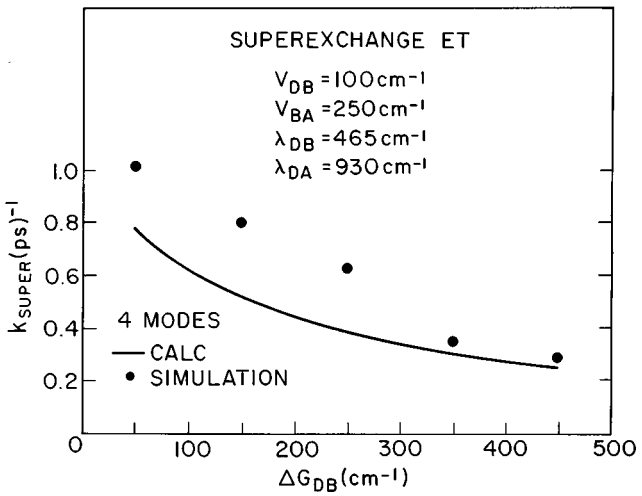

FIG. 7. The energy-gap (ΔG_{DB}) dependence of the superexchange ET rate k_{SUPER} from the electronic origin of DBA obtained from the kinetic fit of the simulated $P_D(t)$ and $P_A(t)$ curves (Fig. 6). Four-mode system (Sec. III) with electronic and nuclear couplings are marked on the figure. The simulated superexchange rate (●) (at each $\Delta G_{DB}>0$) is compared with the calculated (—) quantum mechanical k_{SUPER} rate, Eqs. (5.7) and (5.2).

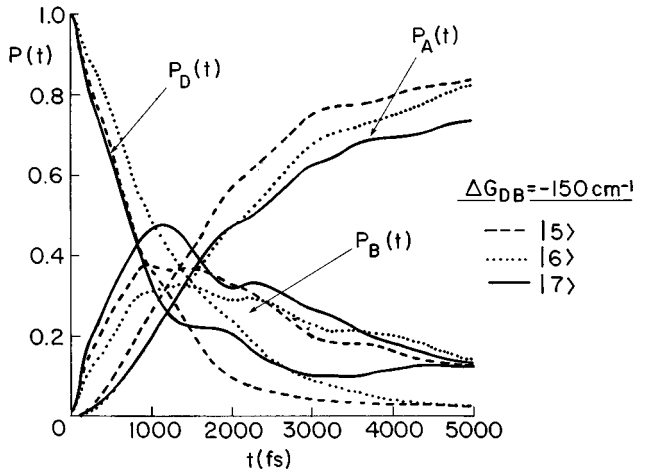

FIG. 8. Mode-specific sequential ET dynamics ($\Delta G_{DB}=-150\ \mathrm{cm}^{-1}$ and $0<E_\alpha\leqslant 108\ \mathrm{cm}^{-1}$). A four-mode system with frequencies $\upsilon_1=27\ \mathrm{cm}^{-1}$, $\upsilon_2=35\ \mathrm{cm}^{-1}$, $\upsilon_3=75\ \mathrm{cm}^{-1}$, and $\upsilon_4=117\ \mathrm{cm}^{-1}$, with the reduced displacements Δ and the nuclear coupling parameters specified in Sec. III. The electronic couplings are $V_{DB}=25\ \mathrm{cm}^{-1}$ and $V_{BA}=35\ \mathrm{cm}^{-1}$. Quantum simulations of $P_D(t)$, $P_B(t)$ and $P_A(t)$, Eq. (2.8), are given for three doorway states: $|\alpha\rangle=|5\rangle[\nu_1+\nu_2]$ ($E_\alpha=62\ \mathrm{cm}^{-1}$) (---), $|\alpha\rangle=|6\rangle[2\nu_2]$ ($E_\alpha=70\ \mathrm{cm}^{-1}$) (....) and $|\alpha\rangle=|7\rangle[\nu_3]$ ($E_\alpha=75\ \mathrm{cm}^{-1}$) (—).

$\Delta G_{DB}=50-450\ \mathrm{cm}^{-1}$. The fluctuations in the population probabilities just reflect the characteristics of the finite system of $n_\alpha+n_\beta+n_\gamma\leqslant 3000$ states, and do not have any physical significance. For the off-resonance couplings, the population probability of the mediating D^+B^-A quasicontinuum is finite and small (e.g., $P_B(t=0)\leqslant 0.03$, Fig. 6), decreasing with increasing ΔG_{DB} (at constant V_{DB}, V_{BA}), and remaining time independent (Fig. 6). This minor constant contribution of $P_B(t)$ reflects the initial preparation conditions of the nonstationary doorway state $|\overline{\alpha}\rangle$ ($\equiv|0\rangle$) of DBA, which includes a contribution to the off-resonance mixing of the $D^+B^-A\{|\beta\rangle\}$ quasicontinuum states, manifesting the finite energy width of the excitation pulse. Such features of the initial conditions for off-resonance coupling in a three electronic levels system were previously noted.[46,47]

The population probabilities $P_D(t)$ and $P_A(t)$ of the initial DBA doorway state and the final D^+BA^- quasicontinuum, respectively, exhibit an exponential decrease of $P_D(t)$ and an exponential increase of $P_A(t)$. The population probabilities can be well described by the direct kinetic scheme mechanism, Eq. (1.2).

$$P_D(t)=\exp(-k_{\mathrm{SUPER}}t), \tag{4.2a}$$

$$P_A(t)=1-\exp(-k_{\mathrm{SUPER}}t). \tag{4.2b}$$

The analysis of the simulations over a broad range of ΔG_{DB} values (Fig. 6) results in the superexchange ET rates k_{SUPER} which are presented vs ΔG_{DB} in Fig. 7. From this analysis we conclude that:

(1) Off-resonance doorway $|\alpha\rangle$-quasicontinuum $\{|\beta\rangle\}$ coupling, in conjunction with off-resonance $\{|\beta\rangle\}$–$\{|\gamma\rangle\}$ inter-quasicontinua coupling results in superexchange unistep kinetics.

(2) Making contact with experiment, we note that superexchange kinetics prevails for the three electronic states system, which satisfies the following conditions: (i) DBA–D^+B^-A off-resonance coupling and (ii) sufficiently high density of states in the final D^+BA^- $\{|\gamma\rangle\}$ manifold to insure $|\alpha\rangle$–$\{|\gamma\rangle\}$ decay in the statistical limit. These simulations concur with the well-known features of superexchange ET kinetics.[6–19,35,41]

C. Mode specific ET dynamics

Up to this point we have been concerned with the simulations of the time development of the initial doorway state, which corresponds to the electronic origin of the DBA manifold. It is of interest to explore ET dynamics from other initial $|\alpha\rangle$ doorway states. We have performed such simulations for the $|\alpha\rangle$–$\{|\beta\rangle\}$–$\{|\gamma\rangle\}$ resonant coupling with a fixed value of $\Delta G_{DB}=-150\ \mathrm{cm}^{-1}$, climbing up the vibrational doorway states manifold in the energy range $E_\alpha=0-108\ \mathrm{cm}^{-1}$. Figure 8 shows typical data for the time-dependent population probabilities, Eq. (2.8), for different initial doorway states $|\overline{\alpha}\rangle$. The dynamics for each $|\overline{\alpha}\rangle$ is sequential, being well represented by Eq. (4.1). The dependence of the lifetimes $\tau_{DA}=(k_{DA})^{-1}$ for the decay of the doorway states manifold (Fig. 9) reveals a modest and irregular E_α dependence with τ_{DA} decreasing by a numerical factor of $\sim$3.5 over this narrow energy range. A detailed analysis of these mode-specific ET rates will be presented in Sec. V.

The simulations of the dynamics established the distinct ET mechanism, i.e., sequential or superexchange, for the decay of a single vibronic level within the DBA manifold. The analysis of the simulations (Figs. 4 and 6) provided the ET rates, i.e., k_{DB}, k_{BA}, and k_{AB} for the sequential mechanism (Fig. 5) and k_{SUPER} for the superexchange mechanism (Fig.

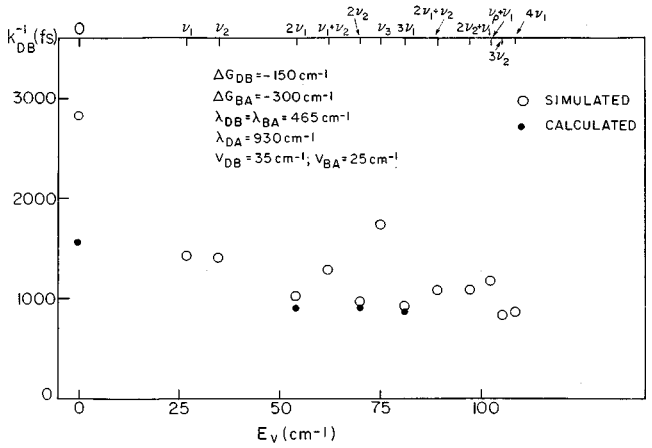

FIG. 9. Mode-selective sequential ET rates k_{DB} in the energy range $E_\alpha = 0-108\ \mathrm{cm}^{-1}$ for a four-mode system specified in Fig. 7 with $\Delta G_{DB} = -150\ \mathrm{cm}^{-1}$. The simulated k_{DB} rates obtained from the analysis of the results of Fig. 7 (and similar data) are compared with the calculated rates (●) using Eqs. (5.1a) and (5.2a).

7). These rates will now be confronted with microscopic ET quantum-mechanical rates calculated from the theory of nonadiabatic ET.

V. MICROSCOPIC ET RATES

A. Formulas

We shall provide explicit quantum-mechanical microscopic rate constants for the sequential kinetic scheme, Eqs. (1.1) and (4.1), and for the superexchange kinetic scheme, Eqs. (1.2) and (4.2). For the sequential $\Delta G_{DB}<0$ mechanism, the rate constants are given by[35,58]

$$k_{DB}=(2\pi/\hbar)V_{DB}^2 FD_{DB}(E_{\overline{\alpha}};E_{\overline{\alpha}}-\Delta G_{DB}), \tag{5.1a}$$

$$k_{BA}=(2\pi/\hbar)V_{BA}^2 AFD_{BA}(E_{\overline{\alpha}}-\Delta G_{DB};E_{\overline{\alpha}}-\Delta G_{DA}), \tag{5.1b}$$

$$k_{AB}/k_{BA}=\rho_B(E_{\overline{\alpha}}-\Delta G_{DB})/\rho_A(E_{\overline{\alpha}}-\Delta G_{DA}), \tag{5.1c}$$

where ρ_B and ρ_A are the densities of states in the D^+B^-A and D^+BA^- manifolds, respectively. For the coupling between a single doorway state $|\overline{\alpha}\rangle$ and the $\{|\beta\rangle\}$ quasicontinuum, the nuclear contribution to the rate (5.1a) is given by the Franck–Condon density,[59] Eq. (3.4), i.e.,

$$FD_{DB}(E_\alpha;E_\beta)=(\delta E)^{-1}\sum_\beta |f(\alpha,\beta)|^2. \tag{5.2a}$$

The β sum is taken over the quasicontinuum states in the energy range δE around $E_{\overline{\alpha}}$. For the $\{|\beta\rangle\}$–$\{|\gamma\rangle\}$ interquasicontinua coupling the nuclear contribution to the rate, Eq. (5.1b), is given by the average Franck–Condon density[59]

$$AFD_{BA}(E_{\overline{\alpha}}-\Delta G_{DB};E_{\overline{\alpha}}-\Delta_{DA})$$

$$=(N\delta E)^{-1}\sum_\beta \sum_\gamma |f(\beta;\gamma)|^2, \tag{5.2b}$$

where the γ sum is taken over the quasicontinuum states $|\gamma\rangle$ within the range δE around $|\beta\rangle$, while the β sum is taken over N states quasidegenerate with $|\overline{\alpha}\rangle$ in the energy range δE. Finally, $\rho_A(E_\gamma)$ and $\rho_D(E_\beta)$ in Eq. (5.1c) are the densities of states in the final D^+BA^- and in the mediating D^+B^-A manifolds, respectively.

Next, we consider the expression for the superexchange kinetic scheme, Eqs. (1.2) and (4.4). For the superexchange mechanism ($\Delta G_{DB}>0$) the rate constant is calculated from a perturbative scheme for the mediated coupling. The approximate expressions for the superexchange coupling are obtained from the first-order mixing of the mediated D^+B^-A $\{|\beta\rangle\}$ states into the doorway data DBA $|\alpha\rangle$. The first-order initial vibronic state (denoted by $|\tilde{\alpha}\rangle$) is

$$|\tilde{\alpha}\rangle=|\alpha\rangle+\sum_\beta |\beta\rangle \frac{V_{DB}f(\beta;\alpha)}{E_\beta-E_\alpha+\Delta G_{DB}}, \tag{5.3}$$

where $f(\beta;\alpha)$ denotes the vibrational overlap integral between the corresponding states, Eq. (2.3).[60]

The DBA$|\tilde{\alpha}\rangle$–$D^+BA^-\{|\gamma\rangle\}$ coupling terms are obtained from Eqs. (2.10) and (5.3)

$$\langle\tilde{\alpha}|\mathbf{H}|\gamma\rangle=V_{DB}V_{BA}\sum_\beta \frac{f(\alpha;\beta)f(\beta;\gamma)}{E_\beta-E_\alpha+\Delta G_{DB}}. \tag{5.4}$$

We now invoke the average energy denominator approximation, i.e., representing the energy gap in Eq. (5.4) by an average value $\overline{E_\beta-E_\alpha}=\lambda_{BD}-E_\alpha$, which corresponds to those β vibronic state(s) with maximal $f(\alpha;\beta)$ vibrational overlap. Using the completeness relation $\Sigma_\beta f(\alpha;\beta)f(\beta;\gamma)=f(\alpha;\gamma)$ one obtains

$$\langle\tilde{\alpha}|H|\gamma\rangle\cong V_{DB}V_{BA}\frac{f(\alpha;\gamma)}{\Delta G_{DB}+\lambda_{BD}-E_\alpha}. \tag{5.5}$$

The superexchange rate k_{SUPER} which appears in Eq. (1.2) is

$$k_{\mathrm{SUPER}}=(2\pi/\hbar)\sum_\gamma |\langle\tilde{\alpha}|\underset{\sim}{H}|\gamma\rangle|^2\delta(E_\alpha-E_\gamma). \tag{5.6}$$

Making use of Eq. (5.5) and of the definition of the averaged spectral density[59] one obtains

$$k_{\mathrm{SUPER}}=(2\pi/\hbar)\frac{V_{DB}^2V_{BA}^2}{(\Delta G_{DB}+\lambda_{BD}-E_\alpha)^2} \times FD_{DA}(E_\alpha;E_\alpha-\Delta G_{DA}), \tag{5.7}$$

where the Franck–Condon density FD_{DA} is given by an expression analogous to Eq. (5.2a). To complete the analysis we require explicit expressions for the Franck–Condon densities,[59] which determine the magnitude of the sequential rates, Eq. (5.1), and of the superexchange rate, Eq. (5.7).

In the calculation and analysis of the quantum mechanical microscopic ET rates, Eqs. (5.1) and (5.7), we have taken both sequential and superexchange rates to be nonadiabatic, i.e., $k_{DB}\propto V_{DB}^2$ and $k_{\mathrm{SUPER}}\propto (V_{DB}V_{BA})^2$. A sufficient validity condition for nonadiabatic dynamics pertains to the absence of interference effects in the decay of DBA$|\alpha\rangle$ resonances.[52] For dynamics in Franck–Condon quasicontinua these interference effects are weak in view of the small, though finite, correlations for $\{|\alpha\rangle\}$–$\{|\beta\rangle\}$ coupling (i.e., small values of the majority of the correlations $|\eta_{\alpha\alpha'}|$) in the vicinity of the electronic origin of the doorway state manifold

TABLE I. Spectral densities. $\Delta G_{DA} = -450\ \mathrm{cm}^1$ and $\Delta G_{BA} = \Delta G_{DA} - \Delta G_{DB}$. Vibrational frequencies and reduced displacements are given in the text. The FD_{DB} and AFD_{BA} data are given for $\Delta G_{DB} < 0$. The FD_{DA} is given for the $\Delta G_{DB} > 0$ data.

ΔG_{DB} cm^{-1}	$FD_{DB}(0, -\Delta G_{DB})$ 10^{-3} cm	$AFD_{BA}(-\Delta G_{DB}; -\Delta G_{DA})$ 10^{-3} cm	ρ_A/ρ_B
−450	2.26	0.53	1
−350	2.12	0.71	1.88
−250	1.00	1.0	4.0
−150	0.43	1.5	12
50–450	$FD_{DA}(0,\Delta G_{DA}) = 2.68 \times 10^{-4}$ cm		⋯

$\{|\alpha\rangle\}$ (Sec. III). A sufficient condition for the lack of interference is expected to be of the form[52] $(\hbar/2)\times(k_\alpha k_{\alpha'})^{1/2}|\eta_{\alpha\alpha'}| \lesssim \hbar\omega$, where k_α and $k_{\alpha'}$ are microscopic decay rates for neighboring $\{|\alpha\rangle\}$ states and ω is a characteristic frequency. Accordingly, $k_{DB}|\eta_{\alpha\alpha'}| \lesssim 2\pi c\omega\ [\mathrm{cm}^{-1}]$ for sequential ET and $k_{\mathrm{SUPER}}|\eta_{\alpha\alpha'}| \lesssim 2\pi c\omega\ [\mathrm{cm}^{-1}]$ for superexchange ET. These relations are reasonably well obeyed for the simulated ET rates (Figs. 5 and 7) with the electronic couplings used herein and with the characteristic frequencies in the range $\omega = 27\text{–}115\ \mathrm{cm}^{-1}$ (i.e., $2\pi c\omega = 2.4\text{–}11\ \mathrm{ps}^{-1}$).

B. Franck–Condon densities

These densities, Eq. (5.2a), and averaged densities, Eq. (5.2b), determine the ET rates, Eqs. (5.1) and (5.7). The Franck–Condon densities $FD_{DB}(E_\alpha;E_\beta)$ for the sequential rate k_{DA}, Eq. (5.1a), and $FD_{DA}(E_\alpha;E_\gamma)$ for the superexchange rate, Eq. (5.7), correspond to the coupling between the doorway state $|\alpha\rangle$ and the vibronic manifolds $\{|\beta\rangle\}$ at $\{E_\beta\} \cong E_\alpha$, or $\{|\gamma\rangle\}$ at $\{E_\gamma\} \cong E_\alpha$, respectively. The Franck–Condon densities, Eq. (5.2a), were calculated using two approaches:

(I) Using the results of a direct calculation of Franck–Condon integrals averaged over a small energy interval ($\delta E = 1\text{–}10\ \mathrm{cm}^{-1}$), according to Eq. (5.2a);

(II) Using the saddle point calculations.[61]

The average Franck–Condon density between the two vibronic manifolds $\mathrm{D}^+\mathrm{B}^-\mathrm{A}\{|\beta\rangle\}-\mathrm{D}^+\mathrm{BA}^-\{|\gamma\rangle\}$ at energies $E_\beta = -\Delta G_{DB}$ and $E_\gamma = -\Delta G_{DA}$ were calculated as follows. For the first few vibronic states in the $\{|\beta\rangle\}$ manifold we used a direct summation according to Eq. (5.2b). When the two manifolds are dense we used the classical approximation[59]

$$AFD_{BA}(E_\beta;E_\gamma) = \frac{\Gamma(n)}{(4\pi\lambda_{BA})^{1/2}\Gamma(n-1/2)} \times \frac{(-\Delta G_{DB}-E_A)^{n-3/2}}{(-\Delta G_{DB})^{n-1}}, \tag{5.8}$$

where $n(=4)$ is the number of the vibrational modes, λ_{BA} is the reorganization energy and $E_A = (\Delta G_{BA}+\lambda_{BA})^2/4\lambda_{BA}$ is the classical activation energy.

In Table I we present some data for FD_{DB} $(E_\alpha = 0;\ E_\beta = -\Delta G_{DB})$ and AFD_{BA} $(E_\beta = -\Delta G_{DB};\ E_\gamma = -\Delta G_{DA})$ densities for the resonance coupling situation ($\Delta G_{DB} = -450$ to $-150\ \mathrm{cm}^{-1}$) of Fig. 4 and for FD_{DA} $(E_\alpha = 0;\ E_\gamma = -\Delta G_{DA})$ for the off-resonance coupling situation of Fig. 6. The values of FD_{DB} $(0; -\Delta G_{DB})$ decrease with decreasing $|\Delta G_{DB}|$, as expected for the normal domain of ET.[2] The AFD_{BA} $(-\Delta G_{DB}; -\Delta G_{DA})$ data correspond to vibrational overlap between high vibrational states in both quasicontinua and their increase with decreasing $|\Delta G_{DB}|$ can be rationalized in terms of the semiclassical expression, Eq. (5.8). These spectral densities will be used for the calculation of the microscopic rates.

C. Rates for sequential and superexchange ET

The quantum-mechanical microscopic rates for sequential ET and for superexchange ET, given in Sec. (5 A), were used since the 1970's for the analysis of experimental ET data and for the quantification of ET dynamics.[62] To assess the reliability and accuracy of these microscopic rates we compare the ET rates calculated from Eqs. (5.1a), (5.1c), and (V.2) and from Eqs. (5.7) and (5.2a) (referred to as ''calculated rates'') with the corresponding results of the simulations based on the radiationless transitions theory of Sec. IV (referred to as ''simulated rates'').

For sequential ET we compare in Fig. 5 the calculated rates k_{DB}, k_{BA}, and k_{AB}, obtained from Eqs. (5.1a), (5.1c), and (5.2), together with the data of Table I, with the simulated rates. The overall agreement is good. For $\Delta G_{DB} = -450$ to $-250\ \mathrm{cm}^{-1}$ the agreement between the calculated and the simulated ET rates is better than 20%, while for the lowest energy gap $\Delta G_{DB} = -150\ \mathrm{cm}^{-1}$ the difference between the calculated and simulated k_{DB} is a numerical factor of 2, originating from the fluctuations of the individual Franck–Condon factors due to the relatively low density of states in the $\mathrm{D}^+\mathrm{B}^+\mathrm{A}$ $\{|\beta\rangle\}$ manifold in this case. For low energy gaps ($\Delta G_{DB} = -150\ \mathrm{cm}^{-1}$), the calculated and the simulated microscopic ET rates from mode selected initial doorway states (Fig. 9) differ by a numerical factor of $\lesssim 2$. This discrepancy reflects again the limitations of our four-mode model for low-energy gaps, which will be removed (in principle) by incorporating a large number of (low-frequency) vibrational modes. Some other features of the sequential kinetics are confirmed by comparison between the calculated and the simulated ET rates. By changing the electronic coupling strengths we find that for the simulated rates $k_{DB} \propto V_{DA}^2$ and $k_{BA} \propto V_{BA}^2$, in accord with Eqs. (5.1a) and (5.1b), while changing the ratio ρ_A/ρ_B of the densities of states we find the asymptotic long-time ratio $P_A(\infty)/P_B(\infty)$

$=\rho_A/\rho_B$, in accord with Eq. (4.1c). We conclude that the nearly quantitative agreement between the calculated microscopic rates and the simulated results confirms the general features of sequential ET (and other nonradiative) dynamics in the Franck–Condon system with two quasicontinua.

For a superexchange ET rate, calculated from Eq. (5.7) and Table I, the agreement between the calculated and the simulated k_{SUPER} rates is good within 10%–40% (Fig. 7). The deviation between the simulated and the calculated k_{SUPER} (Fig. 7) is larger (20%–40%) for small values of $\Delta G_{DB} = 50-250\ \mathrm{cm}^{-1}$ (where $\Delta G_{DB}<\lambda_{DB}$) reflecting the limitation of the average energy denominator approximation. For larger values of ΔG_{DB} ($350-450\ \mathrm{cm}^{-1}$, i.e., $\Delta G_{DB} \sim \lambda_{DB}$) the calculated data converge to the simulated value. The approximate average gap (ΔG_{DB}) dependence of the simulated superexchange rate $k_{\mathrm{SUPER}} \propto (\Delta G_{DB}+\lambda_{DB})^{-2}$ is well obeyed by the data (Fig. 7), in accord with Eq. (5.7). The variation of the electronic coupling terms reveals that for the simulations $k_{\mathrm{SUPER}} \propto (V_{DB}V_{BA})^2$, as expected from Eq. (5.7). It is instructive to note that Eq. (5.7), which rests on the mean energy denominator approximation, provides a reasonably good description of the ET dynamics.

VI. CONCLUDING REMARKS

We have been concerned with ET from a single DBA$|\overline{\alpha}\rangle$ doorway state in the three electronic states DBA–D^+B^-A–D^+BA^- system, determining the energetic control of sequential vs superexchange ET. Simulations of ET dynamics established that ET dynamics from a single doorway vibronic level, which corresponds to the electronic origin of the DBA manifold, over a broad range of ΔG_{DB} values, corresponds either to the sequential ($\Delta G_{DB}<0$) or to the superexchange ($\Delta G_{DB}>0$) mechanism. For the superexchange mechanism, the fate of the final states in the D^+BA^- quasicontinuum (i.e., the subsequent decay) is irrelevant, as the density ρ_A of final states is sufficient to insure irreversible nonradiative relaxation. For the sequential mechanism, the nature of the ET dynamics is also invariant with respect to dephasing processes within the mediating D^+B^-A quasicontinuum, reflecting the characteristics of the (weakly correlated) coupling between the Franck–Condon quasicontinua.

Our treatment rests on the exact diagonalization of the entire Hamiltonian of the system, without considering separation of the relevant system and the bath. In this context, the medium-induced vibrational relaxation and dephasing processes are, in principle, in our formalism. From the point of view of general methodology, we do not claim that vibrational relaxation does not prevail in the mediating D^+B^-A manifold, but rather that sequential mechanism does not require this process. In practice we treated a four-mode system, while other degrees of freedom were not incorporated. Indeed, a four-mode harmonic system is of sufficient size to provide the pertinent information on the ET mechanism. These other degrees of freedom are not explicitly included (in particular, low frequency medium modes) and can be considered as a bath which will contribute to intrastate relaxation and dephasing. In the context of the interplay between intrastate vibrational relaxation between different $|\alpha\rangle$ states in the DBA manifold and their nonradiative nonadiabatic interstate $|\alpha\rangle \rightarrow \{|\beta\rangle\} \rightarrow \{|\gamma\rangle\}$ decay, the population probability $P_D(t)$ has to be extended to incorporate microscopic nonadiabatic rates k_α for different communicating $|\alpha\rangle$ states. In many cases of interest for femtosecond ET dynamics the excess energy (E_α) dependence of k_α is weak, as is the situation for activationless ET.[59] A well-known example is the activationless primary rate for ET from ^{1}P*BH in the native bacterial photosynthetic reaction center.[63] Under these circumstances the effect of the intrastate relaxation in the initial DBA manifold is not important.[59] Regarding additional hidden assumptions in our treatment, we note that the harmonic model employed herein retains the nature of the individual vibrational modes, while anharmonicity effects will induce intrastate vibrational energy redistribution (IVR). IVR effects in ET were considered only in a phenomenological way[59] and deserve further exploration.

To explore further the transition from the sequential to the superexchange ET from a single DBA($|\overline{\alpha}\rangle = |0\rangle$) doorway state, we focus on the energy gap (ΔG_{DB}) dependence of the decay time τ_D of the initial state, i.e., $P_D = \exp(-t/\tau_D)$, where $\tau_D = k_{DB}^{-1}$, Eq. (5.1), for sequential ET and $\tau_D = k_{\mathrm{SUPER}}^{-1}$, Eq. (5.7), for superexchange ET. In Fig. 10

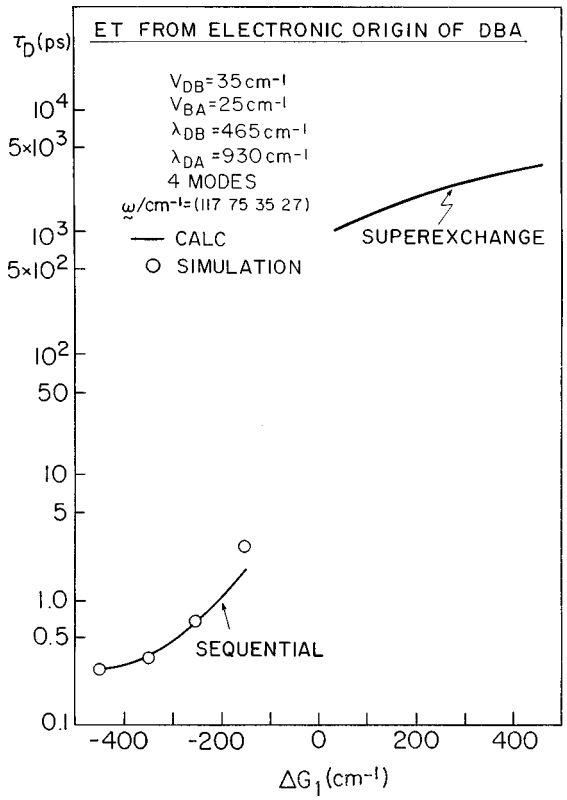

FIG. 10. The energy gap (ΔG_{DB}) dependence of the decay time of the doorway $|\alpha\rangle=|0\rangle$ state (i.e., $\tau_D = k_{\mathrm{SUPER}}^{-1}$ for superexchange ET). The frequencies, electronic coupling, and nuclear coupling are marked on the figure and presented in Sec. III. For sequential ET the results of both quantum-mechanical simulations (○) and calculations (—) of k_{DB}^{-1} are presented. For superexchange ET, k_{SUPER}^{-1} was calculated from Eq. (5.7) with the appropriate electronic couplings [i.e., scaling the results of Fig. 7 by $(V_{DB}V_{BA})^2$].

we present the energy gap dependence of τ_D for the four-mode nuclear parameters specified in Sec. IV, with the electronic coupling parameters $V_{DB}=25\ \mathrm{cm}^{-1}$ and $V_{BA}=35\ \mathrm{cm}^{-1}$. The two branches of the energy-gap dependence (Fig. 10) correspond to the sequential and to the superexchange ET. These nuclear parameters correspond to activationless ET (at $T=0$) for the lowest $\Delta G_{DB}=-450\ \mathrm{cm}^{-1}$, with decreasing the FD_{DB} and increasing τ_D^{SEQ} $(=k_{DB}^{-1})$ in the negative ΔG_{DB} domain. In the positive ΔG_{DB} domain the increase of τ_D^{SUPER} $(=k_{\mathrm{SUPER}}^{-1})$ with increasing ΔG_{DB} reflects the contribution of the energy gap to the electronic coupling, while the FD_{DA} is constant. The dramatic increase of the rates τ_D^{-1} from the superexchange region $(\Delta G_{DB}^{\mathrm{SUPER}}>0)$ to the sequential region $(\Delta G_{DB}^{\mathrm{SEQ}}<0)$, according to Eqs. (5.1) and (5.7), is given by

$$r=(1/\tau_D^{\mathrm{SEQ}})/(1/\tau_D^{\mathrm{SUPER}})=\frac{V_{DB}^2 FD_{DB}}{\left(\dfrac{V_{DB}V_{BA}}{\Delta G_{DB}^{\mathrm{SUPER}}+\lambda_{DB}}\right)^2 FD_{DA}}, \tag{6.1}$$

where on the rhs of Eq. (6.1) $\Delta G_{DB}^{\mathrm{SUPER}}>0$. The ratios of the Franck–Condon densities (Table I) are in the range $f=FD_{DB}/FD_{DA}=1.5-8$. The ratio of the decay rates for the sequential mechanism and for the superexchange mechanism, Eq. (6.1), is $r=[(\Delta G_{DB}^{\mathrm{SUPER}}+\lambda_{DB})^2/V_{BA}^2]f$. Typical values of $\Delta G_{DB}^{\mathrm{SEQ}}=-250\ \mathrm{cm}^{-1}$ and $\Delta G_{DB}^{\mathrm{SUPER}}=250\ \mathrm{cm}^{-1}$, together with the data of Fig. 10, result in $r\cong 3\cdot 10^3$.

Our model simulations, with the parameters used herein, leave an undefined region (''ignorance gap'') in the range $\Delta G_{DB}=-150-50\ \mathrm{cm}^{-1}$, where the nature of the ET mechanism and the behavior of τ_D were not characterized. In the negative ΔG_{DB} domain $-150\ \mathrm{cm}^{-1}<\Delta G_{DB}\leqslant 0$ the breakdown of our simulation scheme reflects the (unphysical) sparse level structure in the mediating $\mathrm{D^+B^-A}\ \{|\beta\rangle\}$ manifold, which will be amended in real life by the large density of (low-frequency) vibrational modes. Holstein's small polaron theory[1(a)] implies that $\tau_D=k_{DA}^{-1}$ for the degeneracy case $\Delta G_{DB}<0$ (also at low T), where the first step in the sequential process involves tunneling with $k_{DB}=V_{DB}^2(FC)_\infty$, with FC_∞ being the appropriate Franck–Condon factor. For the positive gap $(\Delta G_{DB}>0)$ the superexchange coupling, expressed by the perturbative expression, Eq. (5.7), will hold when $|V_{BD}\mathrm{FC}(0;E_\beta)|\ll(E_\beta+\Delta G_{DB})$, where FC is the maximal value of the vibrational overlap between the doorway state and the $\mathrm{D^+B^-A}\ \{|\beta\rangle\}$ manifold at vibrational energy E_β. For the typical parameters used here $\mathrm{FC}\cong 10^{-2}$, and is $V_{DB}=250\ \mathrm{cm}^{-1}$, the resulting inequality is $\Delta G_{DB}\gg 2\ \mathrm{cm}^{-1}$. We thus conclude that in a realistic model system the energetic control of ET prevails over a broad range and only in an extremely narrow energy domain around $\Delta G_{DB}\cong 0$ some deviations will be exhibited. For all practical purposes the characterization of the sequential rate, Eq. (5.1), for $\Delta G_{DB}<0$ and of the superexchange rate, Eq. (5.7), for $\Delta G_{DB}\gg 0$, constitutes an adequate interpolation formula in the undefined region. This analysis also applies for the decay of a vibrationally excited $|\alpha\rangle$ doorway state when the energy gap ΔG_{DB} is changed. These considerations can be readily extended to mode-selective ET dynamics from a single vibronic state $|\alpha\rangle$ in a system characterized by a small (fixed) energy gap ΔG_{DB} (which is comparable to a vibrational frequency). Defining a threshold doorway state $|\overline{\alpha}\rangle$ where $E_{\overline{\alpha}}=\Delta G_{DB}$ we then expect that superexchange ET will occur for $E_\alpha<E_{\overline{\alpha}}$ and sequential ET prevails from vibronic levels with $E_\alpha>E_{\overline{\alpha}}$.

This brings us to the discussion of the parallel sequential-superexchange ET mechanism for the primary charge separation in bacterial photosynthesis.[35,58,64] For a single doorway state the ET mechanism is either sequential (i.e., resonance $\mathrm{DBA}-\mathrm{D^+B^-A}$ coupling) or superexchange (i.e., off-resonance coupling) and no parallel sequential-superexchange mechanism prevails. However, for a system characterized by a fixed $(\Delta G_{DB}>0)$ small energy gap (comparable to the vibrational frequencies) at a finite temperature, the thermally averaged rate for a microcanonical ensemble of the initial $\mathrm{DBA}|\alpha\rangle$ states will result in the superposition of both superexchange and sequential mechanisms for ET from different vibronic levels. These considerations provide justification for the parallel sequential-superexchange mechanism[35,58,64] advanced by us in the context of primary ET in photosynthesis.

We would like to emphasize that our definitions of the sequential vs the superexchange mechanism in terms of the population probabilities $P_D(t)$, $P_B(t)$, and $P_A(t)$, Eq. (2.8), differ from that given by Mukamel *et al.*[49] and by Sumi and Kakitani.[50] The basic difference between our approach and that of Sumi and Kakitani[50] can be realized by considering the following three distinct physical situations:

(I) Off-resonance $\mathrm{DBA}|\alpha\rangle-\{\mathrm{D^+B^-A}|\beta\rangle\}$ coupling, which induces unistep ET, without the population of the $\{\mathrm{D^+B^-A}|\beta\rangle\}$ manifold.

(II) Resonance $\mathrm{DBA}|\alpha\rangle-\mathrm{D^+B^-A}\{|\beta\rangle\}$ coupling, which induces the population of the intermediate $\{\mathrm{D^+B^-A}|\beta\rangle\}$ manifold, with the prevalence of vibrational equilibration in the $\mathrm{D^+B^-A}\{|\beta\rangle\}$ manifold.

(III) Resonance $\mathrm{DBA}|\alpha\rangle-\mathrm{D^+B^-A}\{|\beta\rangle\}$ coupling, which induces the population of the intermediate $\{\mathrm{D^+B^-A}|\beta\rangle\}$ manifold, without vibrational thermalization in the $\mathrm{D^+B^-A}\{|\beta\rangle\}$ manifold.

We characterize situation (I) as superexchange ET and situations (II) and (III) as sequential ET, in contrast to Sumi and Kakitani[50] who attributed situations (I) and (III) to superexchange ET, while situation (II) was assigned to sequential ET. Our physically transparent definitions and analysis of the sequential and the superexchange ET mechanisms are compatible with a long tradition in the areas of physical chemistry and biophysics. Furthermore, our definitions of unistep superexchange and two-step sequential ET via bridges make contact with experimental reality. The interrogation of the time evolution of the population of the $\mathrm{D^+B^-A}\{|\beta\rangle\}$ [without the distinction between situations (II) and (III)] is currently accomplished by time-resolved femtosecond pump–probe spectroscopy.[65] To distinguish experimentally by femtosecond spectroscopy[65] between situations (II) and (III), i.e., the thermally equilibrated $\mathrm{D^+B^-A}$ vibronic manifold and this nonequilibrated manifold at the excess vi-

brational energy of $\sim 500\ \mathrm{cm}^{-1}$ (as is the case for the native photosynthetic bacterial reaction center[35]), is a formidably difficult task, which was not yet accomplished. The physical situation of sequential ET (according to our definition) prior to thermalization in case (III) and in the intermediate situation between cases (III) and (II) are of considerable interest. The issue of competition between ET and vibrational relaxation in the initial and in the intermediate vibronic manifolds were alluded to in the context of primary ET in bacterial photosynthesis[66] and deserve further exploration.

We would like to conclude with a comment on the distinction between the superexchange and sequential mechanisms of ET via bridges. Our definition of case (I) as superexchange and cases (II) and (III) as sequential ET differs from that of Mukamel *et al.*[49] and of Sumi and Kakitani.[50] To avoid semantic pitfalls, we hasten to emphasize that such classifications are meaningful only provided that they are related to experimentally observable properties. Mukamel *et al.*[49] who considered sequential ET proceeding via population of the diagonal elements of the density matrix and superexchange involving electronic coherence contribution, did not provide any predictions regarding the identification of the distinct superexchange and sequential ET mechanisms via bridges, which can be confronted with experimental reality. Sumi and Kakitani[50] considered the distinction between cases (II) and (III), providing an analysis of some implications of vibrational relaxation in the intermediate $D^+B^-A\{|\beta\rangle\}$ manifold. It is still an open question whether these effects can be tested experimentally. Our distinction between superexchange [case (I)] vs sequential [cases (II) and (III)] ET rests on the analysis of the total population probabilities $P_D(t)$, $P_B(t)$, and $P_A(t)$, Eq. (2.8), in conjunction with quantum-mechanical calculations of the microscopic rates. Our apprach provides predictions on the following experimental observables for the primary charge separation in bacterial photosynthesis:[3,35,64,67]

(i) Populations of distinct electronic states. Pump–probe experiments[67] give the time-dependent concentrations of $DBA(P_D(t))$, $D^+B^-A(P_B(t))$, and $D^+BA^-(P_A(t))$. When $P_B(t)$ and $dP_B(t)/dt$ are finite, the sequential mechanism (according to our definition) prevails. In the global analysis of the experimental kinetic data[67] (at all interrogation wavelengths), no distinction was made between the thermalized and nonthermalized $D^+B^-A\{|\beta\rangle\}$ manifolds. Both situations were considered as corresponding to sequential ET, in accord with our analysis.

(ii) The identification of the primary ion-pair state. The experimental interrogation of dichroic excitation spectra of the electric field modulated fluorescence yield from photosynthetic reaction centers identifies the spatial orientation of the dipole moment of the primary ion pair.[68,69] This approach provided a powerful method for the distinction between the two-step sequential ET (via D^+B^-A) and the unistep ET (resulting directly in D^+BA^-). For sequential ET the vectorial information is invariant with respect to the specific vibronic states in the $D^+B^-A|\beta\rangle$ manifold, not distinguishing between cases (II) and (III). This is again in accord with our definitions and analysis.

ACKNOWLEDGMENTS

We are grateful to Professor H. Sumi for stimulating correspondence. This research was supported by the Deutsche Forschungsgemeinschaft (Sonderforschungsbereich 377) and by the Volkswagen Stiftung.

[1] (a) T. Holstein, Ann. Phys. **8**, 325 (1959); **132**, 212 (1981); (b) J. Jortner and S. A. Rice, J. Chem. Phys. **44**, 3364 (1966); (c) H. Sumi, J. Phys. C**17**, 6071 (1984).
[2] R. A. Marcus and N. Sutin, Biochem. Biophys. Acta **811**, 275 (1985).
[3] *The Photosynthetic Reaction Center-Structure and Dynamics*, edited by M. E. Michel-Beyerle (Springer-Verlag, Berlin, 1996).
[4] (a) J. Jortner and M. Bixon, *Ultrafast Phenomena VIII*, edited by J.-L. Martin, A. Mignus, G. A. Mourou, and A. H. Zewail (Springer-Verlag, Berlin, 1993), p. 15; (b) J. Jortner and M. Bixon, Mol. Chryst. Liq. Cryst. **234**, 29 (1993).
[5] (a) N. R. Kestner, J. Logan, and J. Jortner, J. Phys. Chem. **78**, 2148 (1974); (b) M. D. Newton, Chem. Rev. **91**, 767 (1991); (c) M. A. Ratner, J. Phys. Chem. **94**, 4877 (1990).
[6] (a) J. R. Miller and J. N. Beitz, J. Chem. Phys. **74**, 6746 (1981); (b) J. R. Miller, J. N. Beitz, and R. K. Huddleston, J. Am. Chem. Soc. **106**, 5057 (1984); (c) M. D. Johnson, J. R. Miller, N. S. Green, and G. L. Closs, J. Phys. Chem. **93**, 1173 (1989); (d) G. L. Closs, L. T. Calcatterra, N. S. Green, K. W. Penfield, and J. R. Miller, *ibid.* **90**, 3673 (1986).
[7] (a) Edited by T. J. Meyer and M. E. Newton, Chem. Phys. **176**, 289 (1993); (b) Edited by L. G. Arnaut, J. Photochem. Photobiol. A: Chem. **82**, 1 (1994); (c) Edited by M. A. Fox, Chem. Rev. **92**, 365 (1992).
[8] C. A. Stein, N. A. Lewis, and G. Seitz, J. Am. Chem. Soc. **104**, 2696 (1982).
[9] D. Beratan and J. J. Hopfield, J. Am. Chem. Soc. **106**, 1584 (1984).
[10] C. Creitz, Prog. Inorg. Chem. **30**, 1 (1983).
[11] (a) P. Chen, R. Duesing, D. K. Graff, and T. J. Meyer, J. Phys. Chem. **95**, 5850 (1991); (b) J. V. Caspar, B. P. Sullivan, E. M. Kober, and T. J. Meyer, Chem. Phys. Lett. **91**, 91 (1982); (c) J. V. Caspar and T. J. Meyer, J. Am. Chem. Soc. **105**, 5583 (1983); (d) R. S. Lumpkin and T. J. Meyer, J. Phys. Chem. **90**, 5307 (1986); (e) E. M. Kober, J. V. Caspar, R. S. Lumpkin, and T. J. Meyer, *ibid.* **90**, 3722 (1986); (f) K. R. Barqawi, Z. Murzata, and T. J. Meyer, *ibid.* **95**, 47 (1991); (g) L. A. Worl, R. Duesing, P. Chen, L. Della Ciana, and T. J. Meyer, J. Chem. Soc. Dalton Trans. 849 (1991).
[12] (a) E. Akesson, G. C. Walker, and P. F. Barbara, J. Chem. Phys. **95**, 4188 (1991); (b) G. C. Walker, E. Akesson, A. E. Johnson, N. E. Levinger, and P. F. Barbara, J. Phys. Chem. **96**, 3728 (1992).
[13] (a) I. R. Gould, R. H. Young, R. E. Moody, and S. Faris, J. Phys. Chem. **95**, 2068 (1991); (b) I. R. Gould, D. Noukakis, J. L. Goodman, R. H. Young, and S. Farid, J. Am. Chem. Soc. **115**, 3830 (1993); (c) I. R. Gould, D. Noukakis, L. Gomez-Jahn, J. L. Goodman, and S. Farid, *ibid.* **115,** 4405 (1993); (d) I. R. Gould, D. Noukakis, L. Gomez-Jahn, R. H. Young, J. L. Goodman, and S. Farid, Chem. Phys. **176**, 439 (1993).
[14] Y. Zeng and M. B. Zimmt, J. Phys. Chem. **96**, 8395 (1992).
[15] (a) P. Pasman, F. Rob, and J. W. Verhoeven, J. Am. Chem. Soc. **104**, 5127 (1982); (b) H. Oevering, J. W. Verhoeven, M. N. Paddon-Row, and J. M. Warman, Tetrahedron **45**, 4751 (1989); (c) A. M. Oliver, M. N. Paddon-Row, J. Kroon, and J. W. Verhoeven, Chem. Phys. Lett. **191**, 371 (1992); (d) M. Bixon, J. Jortner, and J. W. Verhoeven, J. Am. Chem. Soc. **116**, 7349 (1994); (e) J. W. Verhoeven, T. Scherer, B. Wegewijs, R. M. Harnaut, J. Jortner, M. Bixon, S. Depaemelaere, and F. C. De Schrijver, Rec. des Trav. Chim. des Pays-Bas **114**, 443 (1995).
[16] (a) H. Heitele and M. E. Michel-Beyerle, Chem. Phys. Lett. **134**, 2723 (1987); (b) P. Finckh, H. Heitele, M. Volk, and M. E. Michel-Beyerle, J. Phys. Chem. **92**, 6584 (1988); (c) H. Heitele, Angew. Chem. **32**, 359 (1993); (d) F. Pöllinger, H. Heitele, M. E. Michel-Beyerle, C. Anders, M. Futscher, and H. A. Staab, Chem. Phys. Lett. **198**, 645 (1992); (e) H. Heitele, F. Pöllinger, T. Hüberle, M. E. Michel-Beyerle, and H. A. Staab, J. Phys. Chem. **98**, 7402 (1994).
[17] (a) K. W. Penfield, J. R. Miller, M. N. Paddon-Row, E. Costaris, A. M. Oliver, and N. S. Hush, J. Am. Chem. Soc. **109**, 5061 (1987); (b) H. Oevering, M. N. Paddon-Row, H. Heppener, A. M. Oliver, E. Costaris, J. V. Verhoeven, and N. S. Hush, *ibid.* **109**, 3258 (1987); (c) V. Balaji, L. Ng, K. D. Jordan, M. N. Paddon-Row, and H. K. Patney, *ibid.* **109**, 6957 (1987).

[18] (a) M. R. Wasielewski, M. P. Niemezyk, W. A. Svec, and E. B. Pewitt, J. Am. Chem. Soc. **107**, 1080 (1985); (b) M. R. Wasielewski, Chem. Rev. **92**, 435 (1992).
[19] (a) G. D. Gust and T. A. Moore, Adv. in Photochem. **16**, 1 (1991); (b) G. D. Gust, T. A. Moore, and A. L. Moore, Acct. Chem. Res. **26**, 198 (1993); (c) D. Gust, T. A. Moore, P. A. Liddel, G. A. Nemeth, and I. R. Making, J. Am. Chem. Soc. **109**, 846 (1987); (d) A. N. Macpherson, P. A. Liddel, S. Lin, L. Noss, G. R. Seely, J. M. DeGraziano, A. L. Moore, T. A. Moore, and D. Gust, *ibid.* **117**, 7202 (1995); (e) D. Gust, T. A. Moore, and A. L. Moore, IEEE Engineering in Medicine in Biology (February 1994), p. 58.
[20] S. Nishitani, N. Kurata, Y. Sakata, S. Misumi, and A. Karen, J. Am. Chem. Soc. **105**, 7771 (1983).
[21] G. Tollin, J. K. Hurley, J. T. Hazzard, and T. E. Meyer, Biophys. Chem. **48**, 259 (1993).
[22] O. Farver, S. Wherland, and I. Pecht, J. Biol. Chem. **269**, 22933 (1994).
[23] R. A. Scott, Curr. Biol. **3**, 981 (1995).
[24] J. R. Winkler, B. G. Malmström, and H. B. Gray, Biophys. Chem. **54**, 199 (1995).
[25] (a) J. Kim and D. C. Rees, Nature **360**, 553 (1992); (b) J. Kim and D. C. Rees, Biochemistry **33**, 389 (1994).
[26] (a) A. W. Axup, M. Albin, S. L. Mayo, R. J. Crutchley, and H. B. Gray, J. Am. Chem. Soc. **110**, 435 (1988); (b) J. L. Karas, C. M. Lieber, and H. B. Gray, *ibid.* **110**, 423 (1988); (c) R. Langen, I.-J. Chang, J. P. Germanas, J. H. Richards, J. R. Winkler, and H. B. Gray, Science **268**, 1733 (1995); (d) J. R. Winkler and H. B. Gray, Chem. Rev. **92**, 369 (1992).
[27] O. Farver and I. Pecht, Biophys. Chem. **50**, 203 (1994).
[28] (a) M. P. Jackman, M. L. Lim, G. A. Salmon, and A. G. Sykes, J. Chem. Soc. Chem. Comm. 179 (1988); (b) M. P. Jackman, M. L. Lim, D. J. Salmon, and A. G. Sykes, J. Chem. Soc. Dalton Trans. 2843 (1988); (c) M. P. Jackman, J. McGinnis, R. Powls, G. A. Salmon, and A. G. Sykes, J. Am. Chem. Soc. **110**, 5880 (1988).
[29] G. W. Canters and C. Dennison, Biochimie **77**, 506 (1995).
[30] (a) G. A. Mines, M. J. Bjerrum, M. G. Hill, D. R. Casimiro, I.-J. Chang, J. R. Winkler, and H. B. Gray, J. Am. Chem. Soc. **118**, 1961 (1996); (b) H. B. Gray and J. R. Winkler, Ann. Rev. Biochem. **65**, 537 (1996).
[31] (a) C. J. Murphy, M. R. Arkin, Y. Jenkins, N. D. Ghattia, S. H. Bossmann, N. J. Turro, and J. K. Barton, Science **262**, 1025 (1993); (b) C. J. Murphy, M. R. Arkin, N. D. Ghattia, S. H. Bossmann, N. J. Turro, and J. K. Barton, Proc. Natl. Acad. Sci. USA **91**, 5315 (1994); (c) E. D. A. Stemp, M. R. Arkin, and J. K. Barton, J. Am. Chem. Soc. **117**, 2375 (1995).
[32] S. Priyadarshy, S. M. Risser, and D. N. Beratan, J. Phys. Chem. **100**, 17678 (1996).
[33] (a) *Perspectives in Photosynthesis*, edited by J. Jortner and B. Pullman (Kluwer, Dordrecht, 1989); (b) J. Deisenhofer and J. R. Norris, *The Photosynthetic Reaction Center* (Academic, San Diego, 1993); (c) edited by M. E. Michel-Beyerle and G. L. Small, Chem. Phys. **197**, 223 (1995).
[34] (a) W. Holzapfel, U. Finkele, W. Kaiser, D. Oesterhelt, H. Scheer, H. U. Stilz, and W. Zinth, Chem. Phys. Lett. **160**, 1 (1989); (b) W. Holzapfel, U. Finkele, W. Kaiser, D. Oesterhelt, H. Scheer, H. U. Stilz, and W. Zinth, Proc. Natl. Acad. Sci. USA **87**, 5168 (1990); (c) T. Arlt, S. Schmidt, W. Kaiser, C. Lauterwasser, M. Meyer, H. Scheer, and W. Zinth, Proc. Natl. Acad. Sci. USA **90**, 11757 (1993).
[35] M. Bixon, J. Jortner, and M. E. Michel-Beyerle, Chem. Phys. **197**, 389 (1995).
[36] Y. Jia, T. J. Dimango, C. K. Chan, Z. Wang, M. Du, D. K. Hanson, M. Schiffer, J. R. Norris, G. R. Fleming, and M. S. Popov, J. Phys. Chem. **97**, 13180 (1993).
[37] (a) J. R. Williams, R. G. Alden, H. A. Murchison, J. M. Peloquin, N. W. Woodsbury, and J. P. Allen, Biochemistry **31**, 11029 (1992); (b) H. A. Murchison, R. G. Alden, J. P. Allen, J. M. Peloquin, A. K. W. Taguchi, N. N. Woodsbury, and J. C. Williams, *ibid.* **32**, 3498 (1993).
[38] N. W. Woodsbury, S. Lin, X. Lin, J. M. Peloquin, A. K. W. Taguchi, J. C. Williams, and J. C. Allen, Chem. Phys. **197**, 405 (1995).
[39] M. E. Michel-Beyerle (private communication and to be published).
[40] P. Müller, G. Bieser, G. Hartwich, T. Langenbacher, H. Lossau, A. Ogrodnik, and M. E. Michel-Beyerle (to be published).
[41] M. Plato, M. E. Michel-Beyerle, M. Bixon, and J. Jortner, FEBS Lett. **249**, 70 (1989).
[42] (a) J. Halpern and L. E. Orgel, Disc. Faraday Soc. **29**, 32 (1960); (b) H. A. McConnell, J. Chem. Phys. **35**, 508 (1961).
[43] (a) *Introduction to Molecular Electronics*, edited by M. C. Petty, M. R. Bryce, and D. Bloor (Oxford, New York, 1995); (b) C. A. Mirkin and M. A. Ratner, Ann. Rev. Phys. Chem. **43**, 719 (1992); (c) D. Bloor, Mol. Cryst. Liq. Cryst. **234**, 1 (1992).
[44] (a) J. N. Onuchic and D. N. Beratan, J. Am. Chem. Soc. **109**, 6771 (1987); (b) J. N. Onuchic and D. N. Beratan, J. Chem. Phys. **92**, 722 (1990); (c) D. N. Beratan, J. N. Betts, and J. N. Onuchic, Science **252**, 1285 (1991).
[45] (a) A. M. Kuznetsov and J. Ulstrup, J. Chem. Phys. **75**, 2047 (1981); (b) A. M. Kuznetsov and J. Ulstrup, Chem. Phys. **157**, 25 (1991); (c) Y. I. Kharkats and J. Ulstrup, Chem. Phys. Lett. **182**, 81 (1991); (d) Y. I. Kharkats, A. M. Kuznetsov, and J. Ulstrup, J. Phys. Chem. **99**, 13545 (1995); (e) **99**, 13555 (1995).
[46] (a) R. Egger, C. H. Mak, and U. Weiss, J. Chem. Phys. **100**, 2651 (1994); (b) R. Eggeral and C. H. Mak, J. Phys. Chem. **98**, 9903 (1994).
[47] (a) J. S. Joseph, W. Bruno, and W. Bialek, J. Phys. Chem. **95**, 6242 (1991); (b) J. S. Joseph and W. Bialek, *ibid.* **97**, 3225 (1993).
[48] M. D. Todd, A. Nitzan, and M. A. Ratner, J. Phys. Chem. **97**, 29 (1993).
[49] (a) Y. Hu and S. Mukamel, J. Chem. Phys. **91**, 6973 (1989); (b) O. Kühn, V. Rupasov, and S. Mukamel, *ibid.* **104**, 5821 (1996).
[50] H. Sumi and T. Kakitani, Chem. Phys. Lett. **252**, 85 (1996).
[51] (a) Y. Toyozawa, J. Phys. Soc. Japan **41**, 400 (1976); (b) Y. Toyozawa, A. Kotani, and A. Sum, *ibid.* **42**, 1495 (1977).
[52] (a) M. Bixon and J. Jortner, J. Chem. Phys. (in press); (b) M. Bixon and J. Jortner, *Dynamics in the Franck-Condon Quasicontinuum* (to be published).
[53] (a) W. M. Gelbart, S. A. Rice, and K. F. Freed, J. Chem. Phys. **57**, 4679 (1972); (b) W. M. Gelbart, D. F. Heller, and M. L. Elert, Chem. Phys. **7**, 116 (1975); (c) K. G. Kay, J. Chem. Phys. **61**, 5205 (1974); (d) J. Kommandeur and J. Jortner, Chem. Phys. **28**, 273 (1978); (e) A. Nitzan and J. Jortner, J. Chem. Phys. **71**, 3524 (1979).
[54] (a) J. Jortner, Adv. Laser Spect. **113**, 88 (1977); (b) B. Carmeli and A. Nitzan, Chem. Phys. Lett. **58**, 310 (1978); (c) I. Schek and J. Jortner, J. Chem. Phys. **70**, 3016 (1979); (d) B. Carmeli and A. Nitzan, *ibid.* **72**, 2054, 2080 (1980); (e) B. Carmeli, I. Schek, A. Nitzan, and J. Jortner, *ibid.* **72**, 1928 (1980).
[55] (a) M. Bixon and J. Jortner, J. Chem. Phys. **48**, 715 (1968); (b) M. Bixon and J. Jortner, Israel J. Chem. **7**, 189 (1969); (c) S. Mukamel and J. Jortner, in *MTP International Review of Science*, edited by A. D. Buckingham and C. A. Coulson (Butterworth, London, 1976), Vol. 13, p. 327; (d) J. Jortner and R. D. Levine, Adv. Chem. Phys. **47**, 1, (1981); (e) J. Jortner, in *Femtochemistry*, edited by M. Chergui (World Scientific, Singapore, 1996), p. 15.
[56] F. H. Mies and M. Kraus, J. Chem. Phys. **45**, 4453 (1965).
[57] A. Nitzan and J. Jortner, Mol. Phys. **24**, 109 (1972).
[58] M. Bixon, J. Jortner, M. E. Michel-Beyerle, in *The Photosynthetic Reaction Center—Structure and Dynamics*, edited by M. E. Michel-Beyerle (Springer-Verlag, Berlin, 1996), p. 297.
[59] M. Bixon and J. Jortner, Chem. Phys. **176**, 467 (1993).
[60] We note in passing that some care has to be exerted in the perturbation treatment. We consider the coupling $\mathrm{DBA}|\tilde{\alpha}\rangle$–$\{\mathrm{D^+BA^-}|\gamma\rangle\}$, i.e., between the perturbed first-order doorway state and the zero-order final quasicontinuum. The $\mathrm{DBA}|\tilde{\alpha}\rangle$–$\{\mathrm{D^+BA^-}|\tilde{\gamma}\rangle\}$ coupling with the first-order final quasicontinuum $\{\mathrm{D^+BA^-}|\gamma\rangle\}$ will result in a numerical correction term of ~ 2 for the coupling matrix element, i.e., $\langle \mathrm{DBA},\tilde{\alpha}|\mathbf{H}|\mathrm{D^+BA^-},\tilde{y}\rangle \cong 2\langle \mathrm{DBA},\tilde{\alpha}|\mathbf{H}|\mathrm{D^+BA^-},y\rangle$. The justification for the procedure used herein rests on a self-consistent perturbative solution for the coupling problem $\mathrm{DBA}|\alpha\rangle$–$\mathrm{D^+B^-A}|\beta\rangle$–$\{\mathrm{D^+BA^+}|\gamma\rangle\}$, where the off-resonance quasicontinuum is represented by a single $|\beta\rangle$ level. An analysis (M. Bixon and J. Jortner, unpublished) shows that we should indeed consider the $\langle \mathrm{DBA},\tilde{\alpha}|\mathbf{H}|\mathrm{D^+BA^-},\gamma\rangle$ coupling.
[61] M. Bixon, J. Jortner, J. Cortes, H. Heitele, and M. S. Michel-Beyerle, J. Phys. Chem. **98**, 7289 (1994).
[62] (a) J. Ulstrup and J. Jortner, J. Chem. Phys. **63**, 4358 (1975); (b) S. Efrima and M. Bixon, Chem. Phys. **13**, 447 (1976); (c) J. Jortner and M. Bixon, in *Protein Structure*, edited by R. Austin *et al.* (Springer-Verlag, New York, 1987), p. 277.
[63] M. Bixon and J. Jortner, Chem. Phys. Lett. **159**, 17 (1989).
[64] M. Bixon, J. Jortner, and M. E. Michel-Beyerle, Biophys. Biochim. Acta **1056**, 301 (1991).
[65] (a) *Femtosecond Chemistry*, edited by J. Manz and L. Wöste (VCH, Weinheim, 1995); (b) *Femtochemistry*, edited by M. Chergui (World Scientific, Singapore, 1996).
[66] (a) J. Jortner, Phil. Mag B**40**, 317 (1979); J. Jortner, J. Am. Chem. Soc. **102**, 6676 (1980).

[67] W. Zinth and W. Kaiser, *The Photosynthetic Reaction Center, Vol. II*, edited by J. Deisenhofer and J.R. Norris (Academic, New York, 1993), p. 71.
[68] A. Ogrodnik, U. Eberl, R. Heckmann, M. Kappl, H. Feick, and M. E. Michel-Beyerle, in *Reaction Centers of Photosynthetic Bacteria*, edited by M.E. Michel-Beyerle (Springer-Verlag, Berlin, 1990), p. 157.
[69] D. J. Lockhart, R. F. Goldstein, and S. G. Boxer, J. Phys. Chem. **89**, 1408 (1988).